International Journal of Reliability, Risk and Safety: Theory and Application

Online ISSN: 2676-3346

Vol. 8/ Issue 2/ 2025/ pp. 83-104
DOI: 10.22034/IJRRS.2025.8.2.9
Received: 14 October 2025, Revised: 01 December2025, Accepted: 01 December 2025
Available online at: https://www.ijrrs.com

Original Research Article

A Hybrid FEM–Weibull Framework for Vibration-Induced Fatigue Life Prediction and Reliability Enhancement of Solder Joints in Space-Grade PCB

Amirhosein Rahbar [1] and Seyed Mohammad Navid Ghoreishi [2*]

1. Department of Mechanical Engineering, Sharif University of Technology (SUT), Tehran, Iran

2. Satellite Research Institute, Iranian Space Research Center, Tehran, Iran

*** smn.ghoreishi@isrc.ac.ir**

Abstract

The reliability of space-grade electronic boards is significantly compromised by vibration loads experienced during launch and orbital operations. These mechanical loads accelerate fatigue damage in printed circuit boards (PCBs) and their solder joints. Most existing studies address individual factors and rely on simplified uniaxial analyses, which fail to capture the complex, multidirectional mechanical conditions present in real space environments. This study proposes a unified framework for vibration–fatigue prediction that integrates finite element modeling, frequency-domain stress analysis, and Weibull-based life estimation. The proposed method enables the simultaneous evaluation of loading direction, package type, and solder alloy behavior. A multilayer PCB containing BGA, LCCC, and leaded packages was modeled, and both sinusoidal and random vibration loads were applied. Simulations were conducted under both uniaxial and triaxial excitations. The results reveal key findings. Triaxial loading significantly increases stress levels and uncovers failure modes not identified through uniaxial analysis. Leaded packages demonstrate longer fatigue life due to the compliance of their leads. Among the solder alloys, SAC305 exhibits superior performance compared to Pb90Sn10 and Sn100C. The finite element model directly correlates stress data with statistical life predictions, offering a realistic and quantitative understanding of vibration-induced fatigue. Overall, the proposed method provides a practical and robust tool for designing more reliable space electronics.

Keywords: Solder Joint Reliability; Finite Element Modeling; Weibull Distribution; Vibration Loading; Vibration Induced Fatigue; Aerospace Electronics.

1. Introduction

Electronic systems used in space applications are continuously subjected to mechanical vibrations arising from launch acceleration, orbital correction maneuvers, propulsion events, reaction wheel actuations, and internal mechanical mechanisms. Printed circuit boards (PCBs), which serve as the structural and functional backbone of these systems, are particularly vulnerable to such environments. Under sinusoidal and random excitations, PCBs may undergo dynamic deflection, resonant amplification, and progressive fatigue deterioration, all of which pose critical reliability threats to space missions [1–3].

In area-array and leaded package assemblies, solder joints, especially those connecting BGA, LCCC, and leaded devices, are the most fatigue-prone elements within the interconnect structure, as their mechanical behavior is strongly influenced by vibration amplitude, multiaxial loading, and solder alloy properties [4–7]. These factors govern the development of cyclic stresses, plastic strain accumulation, and crack nucleation at the solder interfaces. The statistical characterization of these dispersion-driven failure mechanisms is commonly performed using Weibull parameters and MTTF-based

How to cite this article:
A.H. Rahbar and S. M. N. Ghoreishi, "A hybrid FEM–Weibull framework for vibration-induced fatigue life prediction and reliability enhancement of solder joints in space-grade PCB," *International Journal of Reliability, Risk and Safety: Theory and Application*, vol. 8, no. 2, pp. 83-104, 2025, doi: 10.22034/IJRRS.2025.8.2.9.

metrics, which offer a probabilistic framework for evaluating vibration-induced fatigue life [8].

The impact of vibration-induced fatigue is particularly significant for space-grade PCBs, where long-duration sinusoidal inputs, often generated by propulsion systems or attitude control maneuvers, are common [9]. Solder joint failure typically initiates at stress-concentrated regions and propagates through microstructural degradation mechanisms such as grain rotation, intergranular crack growth, and intermetallic compound (IMC) layer thickening [10]. Vibration amplitude is a dominant factor influencing the failure mode: low amplitudes promote creep-dominated degradation, whereas high amplitudes accelerate plastic deformation, strain localization, and intergranular fracture [11]. Frequency content also plays a critical role; when excitation aligns with the natural modes of the PCB, local displacements can be amplified by an order of magnitude, significantly increasing stress within solder joints and reducing fatigue life [12–14].

Multiaxial vibration introduces further complexity into solder fatigue behavior. Combined out-of-plane bending, in-plane shear, and torsional components generate mixed-mode stress fields that are inadequately captured by conventional uniaxial analytical models [15]. Recent studies have shown that multiaxial loading can produce equivalent stress levels two to three times higher than those observed under uniaxial excitation, while also altering crack initiation sites and propagation trajectories in BGA, LCCC, and leaded joints [26–33]. These findings underscore the necessity for fatigue prediction frameworks that consider the directionality, phase relationships, and dynamic coupling inherent to aerospace vibration environments.

Amplitude–frequency coupling is another critical factor affecting solder degradation. Higher amplitudes consistently correlate with shorter fatigue lives, especially under resonant conditions. Excitation frequencies between 100 and 500 Hz, commonly encountered during launch, have been identified as particularly damaging to space electronics [16–21]. Solder alloy composition further modulates this behavior. Lead-free SAC alloys exhibit strain-rate sensitivity, viscoelastic response, and microstructural evolution under dynamic loading, while doped SAC variants demonstrate improved resistance to crack initiation and slower IMC formation [22–25]. Often, the interaction between amplitude and frequency determines whether failure modes are creep-dominated or fatigue-dominated, necessitating predictive models that incorporate both effects concurrently [21].

Multiaxial loading has also been shown to accelerate shear-driven failure mechanisms, promote intergranular cracking, and increase damage accumulation by 25–60%, depending on phase coherence and load configuration [26–31]. Both numerical and experimental studies confirm that triaxial excitation, synchronous loading, and torsional inputs significantly affect failure progression, reducing MTTF and shifting dominant fracture paths within solder joints [32–33]. These results reinforce the need for analytical approaches that account not only for amplitude and frequency effects but also for the directional complexity of real spaceflight vibration conditions.

Advanced statistical tools, particularly those based on Weibull distributions, have proven effective in characterizing solder fatigue and estimating lifetime under variable and uncertain conditions [34–37]. Recent developments, including hybrid Weibull models and machine learning–enhanced reliability frameworks, further improve predictive accuracy under amplitude variability, frequency interaction, and small sample sizes [38–41]. Concurrently, package architecture plays a critical role in vibration fatigue behavior. Leaded components offer mechanical compliance that mitigates bending stress; BGA packages provide more uniform stress distribution but are vulnerable to void-induced failure; and LCCC devices experience high interfacial stress concentrations that promote early crack initiation [42–49].

Despite these contributions, a major research gap remains: most prior studies examine vibration amplitude, frequency, multiaxiality, solder alloy characteristics, or package design in isolation. This fragmented approach limits predictive accuracy, as solder fatigue in space environments is fundamentally governed by coupled interactions between dynamic response, material behavior, and multidirectional loading [18,34]. Moreover, current accelerated life test methodologies fail to replicate the true multiphysics vibration environment encountered in actual spacecraft, often yielding non-conservative reliability estimates.

The present study addresses these limitations by introducing a unified, hybrid FEM–Weibull reliability framework that concurrently incorporates dynamic response characteristics, multiaxial vibration loading, solder alloy type (Pb90Sn10, SAC305, Sn100C), and package architecture (BGA, leaded, LCCC). Using frequency-response analysis, modal characterization, and probabilistic life estimation, the proposed methodology bridges the gap between deterministic vibration analysis and stochastic reliability modeling. It offers a comprehensive and mission-relevant framework for evaluating vibration-induced solder fatigue in space-grade PCB assemblies, supporting the development of more robust electronic systems for high-vibration aerospace applications.

2. Theoretical background

2.1 Random Vibration [50]

Random vibration environments encountered in aerospace systems are commonly represented in the frequency domain using the power spectral density (PSD) function $G(f)$, which specifies the distribution of vibrational energy across the

frequency spectrum. The fatigue-relevant stress response of printed circuit boards (PCBs) and solder joints under such stochastic loading conditions can be derived from the spectral moments, expressed as:

$$m_i = \int_{\{0\}}^{\{\infty\}} f^i G(f) df \quad (1)$$

where m_0, m_2, and $m_4$correspond respectively to the stress variance, dominant frequency content, and curvature of the PSD. These parameters allow computation of the zero-crossing frequency and peak occurrence frequency:

$$V_0 = \sqrt{\frac{m_2}{m_0}}, V_P = \sqrt{\frac{m_4}{m_2}}, \quad (2)$$

which are essential for estimating the cyclic content of the random stress field.

To characterize the spread of vibrational energy, bandwidth descriptors such as the narrow-bandness ratio are used, including:

$$\alpha_2 = \frac{m_2^2}{m_0 m_4} \quad (3)$$

Values of α_2 approaching 1 indicates a narrow-band process dominated by resonance, whereas values near 0 represent a wide-band stochastic process. As shown in Table 1, the key PSD-derived parameters used in random vibration fatigue are summarized.

Table 1. Key PSD-Derived Parameters Used in Random Vibration Fatigue

Quantity	Equation	Physical Meaning
Spectral Moment (m_i)	$\int_0^\infty f^i G(f)\, df$	Governs energy, frequency content, curvature
Variance (m_0)		RMS stress level
Zero-Crossing Frequency (V_0)	$\sqrt{m_2/m_0}$	Number of stress cycles per unit time
Peak Frequency (V_P)	$\sqrt{m_4/m_2}$	Expected rate of stress peaks
Bandwidth (α_2)	$m_2^2/(m_0 m_4)$	Narrow-band vs. wide-band classification
Damage Rate (D)	$V_P \int p(S)/N(S), dS$	Rate of fatigue damage accumulation
Fatigue Life (T)	$(1/D)$	Predicted time to failure

Fatigue damage under random vibration is computed using the Palmgren–Miner rule:

$$D = V_P \int_0^\infty \frac{p(S)}{N(S)}\, dS \quad (4)$$

where $p(S)$represents the probability density of the stress amplitude and $N(S) = CS^{-k}$is the material's S–N curve. Correspondingly, fatigue life is obtained as:

$$T = \frac{1}{D} \quad (5)$$

Since the stress-amplitude distribution $p(S)$ is not known a priori, frequency-domain fatigue models (Rayleigh, Wirsching–Light, Tovo–Benasciutti, Dirlik) are employed to approximate $p(S)$ based on PSD-derived parameters. These formulations allow fatigue assessment without time-domain simulations, making them particularly appropriate for aerospace electronics exposed to broadband random vibration. Figure 1 illustrates the frequency-domain fatigue evaluation under random vibration.

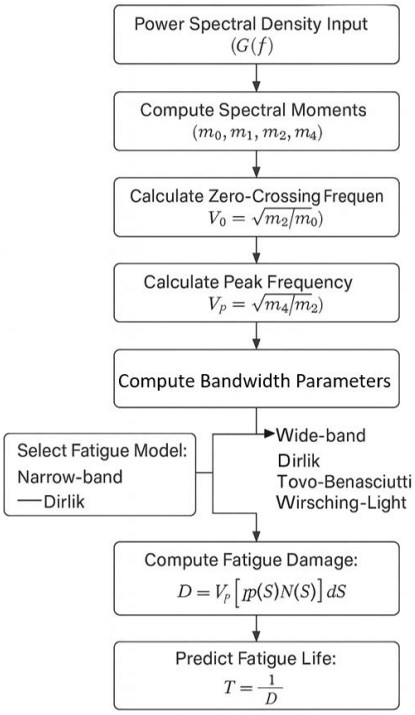

Figure 1. Frequency-Domain Fatigue Evaluation Under Random Vibration

2.1.1 Frequency Domain Methods

Fatigue life prediction under Gaussian random vibration requires the estimation of the probability density function $p(S)$of stress amplitudes, as introduced in Equation (10). Several empirical and semi-empirical formulations have been developed to approximate $p(S)$ using spectral moments derived from the power spectral density (PSD) function. These methods vary in terms of accuracy, computational cost, and their applicability to narrow-band versus wide-band random processes. The following subsections summarize the most widely adopted approaches for vibration-induced fatigue assessment, with an emphasis on their relevance to aerospace structures, where broadband excitation and multi-modal dynamic responses are prevalent.

- Narrow Band Approximation
- Wirsching–Light Method
- Single Moment Method
- Tovo–Benasciutti Method
- Dirlik Method

(1) Narrow Band Approximation

The narrow-band approximation assumes that the stress process is dominated by a single mode with nearly sinusoidal cycles, allowing $p(S)$to be modeled by the Rayleigh distribution:

$$p(S) = \frac{S}{\sigma_s^2} \exp\left(-\frac{S^2}{2\sigma_s^2}\right) p \quad (6)$$

The cumulative damage per unit time can be:

$$D_{NB} = \frac{V_P}{C} m_0^{k/2} \Gamma\left(1 + \frac{k}{2}\right) \quad (7)$$

This formulation is accurate only when $\alpha_2 \approx 1$. When applied to wide-band inputs, it consistently overestimates damage.

(2) Wirsching–Light Method

To reduce narrow-band conservatism in wide-band conditions, Wirsching and Light introduced a correction factor:

$$\lambda_{WL} = a(k) + [1 - a(k)](1 - \epsilon)^{b(k)} \quad (8)$$

where the bandwidth parameter ϵ is defined as:

$$\epsilon = \sqrt{1 - \alpha_2^2} \quad (9)$$

This method improves accuracy for broadband PSDs while retaining computational simplicity, making it suitable for multi-modal aerospace structures.

(3) Single Moment Method

This approximation relies solely on a single moment from the PSD curve, making it computationally lightweight for preliminary vibration fatigue assessments in mechanical systems. Its correlation factor with the narrow band method is:

$$V_{SM} = \left(\frac{m_{2/k}}{m_0}\right)^{k/2} \quad (10)$$

where $\boldsymbol{m_{2/k}}$ is the spectral moment of order 2/k, and k is the material constant from Equation (11). The cumulative damage is expressed as:

$$D_{SM} = D_{NB} \cdot \frac{1}{C} m_0^{k/2} \left(2^{k/2} \Gamma\left(1 + \frac{k}{2}\right)\right) \quad (11)$$

While computationally efficient, the method is best suited for preliminary screening rather than final design of aerospace components.

(4) Tovo–Benasciutti Method

Tovo and Benasciutti proposed a combination of upper and lower bounds of narrow-band damage:

$$\lambda_{TB} = b_1 \alpha_2 + b_2 (1 - \alpha_2) \quad (12)$$

Where α_2 follows Equation (6), and the parameter b is:

$$b = e^{-\alpha_1} [1.112(1 - \alpha_1)^{1.1} + 0.1\alpha_1] b \quad (13)$$

The corrected cumulative damage is:

$$D_{TB} = \lambda_{TB} D_{NB} \quad (14)$$

This method is robust across a wide range of bandwidths and is frequently adopted in vibration fatigue assessments of aerospace components.

(5) Dirlik Method

The Dirlik model provides an empirical expression for $p(S)$based on extensive rainflow simulations:

$$\mathrm{P}(S) = \frac{G_1}{Q} e^{-QZ} + G_2 Z e^{-Z^2} + G_3 Z e^{-Z^2/2} \quad (15)$$

Where Z is the normalized amplitude, the method remains one of the most accurate wide-band formulations and is widely used for the qualification of aerospace hardware under broadband vibration. Table 2 presents a comparison of the different frequency-domain fatigue models.

Table2. Comparison of Frequency-Domain Fatigue Models

Method	Bandwidth Suitability	Accuracy	Computational Cost
Narrow-Band	$\alpha_2 \approx 1$	Medium	Very Low
Wirsching–Light	Moderate–Wide	Medium–High	Low
Single-Moment	Moderate	Low–Medium	Very Low
Tovo–Benasciutti	Wide	High	Medium
Dirlik	Wide	Very High	Medium

2.1.2 Sinusoidal Loading

Sinusoidal vibration provides a deterministic form of excitation and is particularly useful for evaluating resonance amplification in printed circuit boards (PCBs). When the excitation frequency approaches a natural mode of the structure, both displacement and stress levels increase sharply, especially at critical locations such as solder joints and component leads.

Standard sinusoidal vibration tests, including those specified in NASA GEVS, MIL-STD-810, and ECSS, apply frequency sweeps to identify resonant peaks or use fixed-frequency excitation to assess durability under sustained dynamic loading. Unlike random vibration, sinusoidal excitation enables direct cycle counting, offering a more straightforward approach to estimating fatigue life for resonance-dominated failure modes.

Although sinusoidal input does not replicate the broadband characteristics of launch environments, it remains an essential step in model calibration, resonance identification, and validation of finite element method (FEM) responses before conducting random vibration analysis.

2.2 Fatigue Models for Solder Joints under Vibrational Loading

Predicting the fatigue life of solder joints subjected to vibrational loading remains one of the major challenges in the design and qualification of aerospace electronic hardware. Deterministic sinusoidal excitation, primarily associated with resonance-driven cyclic deformation and broadband random vibration typically encountered during launch, handling, and transport, results in repeated stress and strain cycles in solder interconnects. These cycles accumulate damage over time, ultimately leading to fatigue-driven mechanical failure. To characterize and quantify this degradation, several fatigue modeling approaches have been developed, each based on a specific damage parameter such as strain, energy, creep deformation, or cumulative cycle summation.

2.2.1 Strain-Based Models

Among the earliest formulations, the Coffin–Manson relation correlates fatigue life with plastic strain amplitude. Although this model performs well under low-cycle fatigue conditions, its accuracy diminishes under

the high-frequency, multi-modal excitations common in aerospace applications. Frequency-adjusted extensions, such as the Shi model, incorporate excitation frequency into the strain-based formulation and provide improved predictions for high-cycle fatigue regimes. In the context of electronic packaging, Engelmaier's shear strain–based modification offers better correlation with the in-plane shear deformation exhibited by leadless chip carriers (LCCs), ceramic chip carriers (CCCs), and surface-mounted devices. More recent developments in this class of models also consider thermomechanical mismatch effects arising from differences in the coefficients of thermal expansion (CTE) between the package and the PCB.

2.2.2 Temperature- and Frequency-Sensitive Models

Models such as the Norris–Landzberg equation incorporate temperature, cycling frequency, and activation energy to scale accelerated test results to actual operational conditions. This approach has proven particularly useful in mission qualification processes. Syed's model extends this framework by accounting for accumulated creep strain and creep energy density dominant damage mechanisms in ball grid array (BGA) and chip-scale package (CSP) assemblies exposed to thermomechanical vibration and viscoplastic deformation.

2.2.3 Energy-Based Models

Energy-based models assume that fatigue failure occurs when a critical strain energy density or hysteresis energy threshold is exceeded. Notable approaches developed by Manson, Pan, and Kujawski utilize total or plastic strain energy per cycle as the damage metric. These models integrate well with finite element analysis (FEA) frameworks, where strain energy can be directly extracted at solder joints, making them particularly suitable for analyzing complex, multi-axial, and non-proportional vibration loading scenarios.

2.2.4 Creep-Driven and Rate-Dependent Approaches

Solder joints, especially those composed of lead-free alloys such as SAC305, exhibit pronounced viscoplastic and creep-sensitive behavior. Creep-based models, including those proposed by Syed and Wong, quantify damage by evaluating accumulated creep strain or creep work density under coupled temperature–vibration conditions. These models are particularly relevant for high-temperature dwell phases or slow cyclic loads superimposed on vibrational excitation.

2.2.5 Damage Accumulation Models

Empirical models such as Miner's linear damage rule, the Grover model, and the Corten–Dolan modification offer simplified, cycle-by-cycle damage accumulation frameworks. These models are computationally efficient and useful in early design evaluations; however, they lack the ability to capture load sequence effects and nonlinear viscoplastic responses. Nevertheless, they remain widely used in practical applications, especially when large datasets or mixed loading profiles are involved.

2.2.6 Fracture Mechanics–Based Models

Mechanistic approaches, including Darveaux's crack initiation and propagation model and Gustafsson's formulation for lead-free BGAs, provide high-fidelity predictions through explicit modeling of crack evolution at solder interfaces. These models rely on interfacial energy accumulation, viscoplastic strain energy density, and microstructural degradation to estimate both crack initiation life and propagation rate. Although computationally intensive, they offer significantly improved predictive accuracy compared to empirical or cycle-counting approaches, particularly under complex, multi-axial, and dynamic loading conditions. Table 3 provides a summary of the fatigue life prediction models.

Table 3. Summary of fatigue life prediction models

Fatigue Model	Damage Parameter	Package Applied	Required Parameters
Coffin–Manson [51]	Plastic strain	N/A	$\Delta\varepsilon$: plastic strain range; m: fatigue exponent; C: ductility coefficient
Shi [51]	Frequency-modified plastic strain	N/A	$\Delta\varepsilon$: plastic strain range; f: frequency; k: frequency exponent; m: fatigue exponent; C: ductility coefficient
Engelmaier [51]	Shear strain	LCC, CCC	$\Delta\gamma$: cyclic shear strain range; εf: fatigue ductility coefficient; c: fatigue exponent
Engelmaier [51]	Shear strain	Leadless SMD	$\Delta\gamma$: shear strain range; c: fatigue exponent
Engelmaier [51]	Package geometry & temperature	Stiff leadless & leaded SMD	LD: half joint distance; $\Delta\alpha$: CTE difference; β: Weibull parameter; F: empirical factor; ΔT: temperature; ε: ductility coefficient; c: fatigue exponent
Solomon [51]	Shear strain	60/40 solder sheet	$\Delta\gamma$: plastic shear strain range; α, θ: constants
Norris–Landzberg [51]	Temperature & cycle frequency	N/A	ΔT: temperature range; f: frequency; Tmax: max temperature; Q: activation energy; k: Boltzmann's constant
Syed [51]	Accumulated creep strain	PBGA	E: accumulated creep strain; C: creep ductility
Syed [51]	Accumulated creep strain & energy density	BGA, CSP (SAC, SnPb)	εc: accumulated creep strain; Wc: creep energy density; C: creep constant; W: energy constant

Fatigue Model	Damage Parameter	Package Applied	Required Parameters
Manson [51]	Creep & plastic strain	Steel pipe	Δεp: reversed plasticity; Δεpc: plasticity–creep; Δεcp: creep–plasticity; Δεc: reversed creep
Akay [51]	Volume-weighted creep strain	LCC	$\bar{\gamma}$: avg effective creep shear strain; εf: fatigue ductility coefficient; k: fatigue exponent
Akay [51]	Total creep strain energy	LCC	ΔW: strain energy; εf, k: material constants
Knecht & Fox [51]	Creep strain	SMD joints	Δγ: creep strain; C: constants
Stowell [51]	Energy loss	Steel	σf, εf: fracture stress/strain; E, σ0, ε0: constants
Pan [51]	Strain energy density & geometry	LCCC	C: critical strain energy; Wp: plastic energy; Wc: creep energy; a, b: weighting factors
Kujawski [51]	Strain energy density per cycle	Metal	ΔW: elastic strain energy; Wt: total density; C, d: constants
Joseph [51]	Cumulative hysteresis energy	FE model	$\bar{W}$: avg hysteresis energy; Wt: total energy; Wc: dissipated energy per cycle
Morrow [51]	Plastic strain energy density	Metal tubes	Wp: plastic strain energy; m: fatigue exponent; C: ductility coefficient
Solomon [51]	Frequency-modified strain energy density	60/40 solder	Wp: plastic strain energy; v: frequency; k, n: frequency exponents; C: ductility coefficient
Miner [51]	Damage per cycle	N/A	ni: cycles at amplitude; Ni: life at amplitude; m: stress levels
Hamasha [51]	Damage per cycle (stress effect)	Solder joint	ni: cycles (low amp.); Ni: life; n, N: cycles/life at high amp.; fi: hysteresis energy
Darveaux [51]	Crack initiation & propagation	SnPb assemblies	a: crack length; da/dN: growth rate; ΔW: viscoplastic energy; K1–K4: constants
Gustafsson [51]	Crack initiation/propagation	Lead-free BGA	Wc, Nc: crack initiation energy; a: crack length; propagation rates

2.3 The Weibull Distribution Model

The Weibull distribution is one of the most widely adopted statistical models for quantifying fatigue-life variability in electronic solder joints because of its ability to represent early-life failures, random failures, and wear-out phenomena through a unified framework. This flexibility makes the Weibull distribution particularly suitable for vibration-induced fatigue, where failure mechanisms are governed by material scatter, microstructural heterogeneity, and environmental variations.

For a two-parameter Weibull model, the probability density function (PDF) is:

$$f(t;\beta,\eta) = \frac{\beta}{\eta}\left(\frac{t}{\eta}\right)^{\beta-1}\exp\left[-\left(\frac{t}{\eta}\right)^{\beta}\right], \quad t \geq 0 \qquad (16)$$

where **β** is the shape parameter, and **η** is the scale (characteristic life). The cumulative distribution function is:

$$(t;\beta,\eta) = 1 - \exp\left[-\left(\frac{t}{\eta}\right)^{\beta}\right] \qquad (17)$$

The shape parameter β directly indicates the underlying failure mechanism:

- **β < 1:** decreasing failure rate (early defects),
- **β ≈ 1:** constant rate (random failures),
- **β > 1:** increasing rate (wear-out dominated by fatigue).

Solder-joint fatigue under vibration typically yields **β > 1**, consistent with damage accumulation and crack growth under cyclic stresses.

The reliability function is:

$$R(t) = \exp\left[-(\frac{t}{\eta})^{\beta}\right] \qquad (18)$$

And the hazard rate is:

$$h(t) = \frac{\beta}{\eta}(\frac{t}{\eta})^{\beta-1} \qquad (19)$$

Which increases monotonically for β > 1, characteristic of vibrational fatigue.

A key metric for vibration-fatigue reliability is the mean time to failure (MTTF):

$$\text{MTTF} = \eta\,\Gamma(1+\frac{1}{\beta}) \qquad (20)$$

And low-percentile lifetimes (e.g., B10) obtained from the inverse CDF, which are critical for aerospace qualification requirements.

For materials exhibiting a nonzero threshold life or minimum damage accumulation period, the three-parameter Weibull distribution introduces a location parameter γ:

$$f(t) = \frac{\beta}{\eta}(\frac{t-\gamma}{\eta})^{\beta-1}\exp\left[-(\frac{t-\gamma}{\eta})^{\beta}\right], t \geq \gamma \qquad (21)$$

This is useful when describing solder joints that do not fail below certain stress amplitudes.

In vibration-fatigue environments, the Weibull distribution integrates naturally with frequency-domain fatigue damage models. The damage accumulation predicted from PSD-based methods (e.g., Dirlik, Tovo–Benasciutti) provides the cycles-to-failure input for Weibull parameter estimation. This synergistic combination allows mapping simulated vibration severity to a probabilistic lifetime model, enabling the prediction of B-life values and mission-relevant reliability margins.

Parameter estimation challenges include small sample bias, zero-failure datasets, and sensitivity to outliers. MLE, Bayesian estimation, and censored-data techniques provide robust solutions. Goodness-of-fit metrics (e.g., Kolmogorov–Smirnov) are often required for validation.

Overall, the Weibull distribution offers a physically consistent and statistically robust framework for lifetime prediction of solder joints under both sinusoidal and random vibration profiles. Its integration with finite-element-based stress responses and frequency-domain damage metrics provides the probabilistic foundation needed for reliability analysis of space-grade electronic assemblies.

2.4 Solder Fatigue under Vibrations Loading

The fatigue life of printed circuit boards (PCBs) subjected to random vibration is governed by the interaction of (1) structural design parameters, (2) environmental loading conditions, and (3) material properties. These factors influence both the global dynamic response of the board and the local stress–strain behavior at solder joints. As illustrated in **Figure 2**, their coupled effects, especially vibration–thermal interactions, are often responsible for accelerated degradation and early-life failures. Reliable fatigue prediction, therefore, requires a multi-physics understanding supported by finite element analysis (FEM) and standardized qualification procedures such as MIL-STD-810, NASA-GEVS, and ECSS.

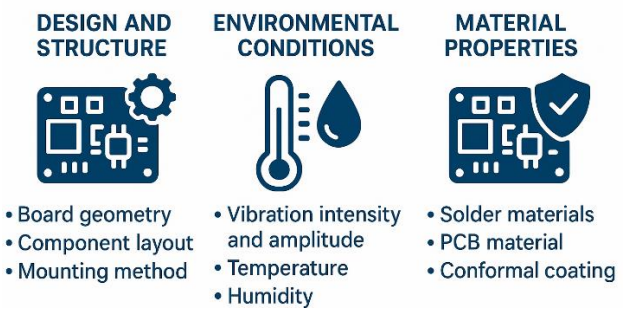

Figure 2. Factors Affecting the Lifetime of an Electronic Board

2.4.1 Design and Structural Factors

Structural configuration directly affects modal behavior and stress distribution in a vibrating PCB. The most influential parameters are board geometry, component arrangement, and mounting strategy, as summarized in **Figure 3**.

- **Board Geometry**

Mass distribution and placement of large components significantly alter local vibration modes. Asymmetric layouts amplify local curvature and shear strain at solder joints, particularly in BGA and LCCC packages. Placing high-mass packages near nodal regions or toward the geometric center produces more uniform load distribution. FEM-based layout optimization has demonstrated fatigue-life improvements approaching a factor of two under severe vibration.

- **Component Layout**

Mass distribution and placement of large components significantly alter local vibration modes. Asymmetric layouts amplify local curvature and shear strain at solder joints, particularly in BGA and LCCC packages. Placing high-mass packages near nodal regions or toward the geometric center produces a more uniform load distribution. FEM-based layout optimization has demonstrated fatigue-life improvements approaching a factor of two under severe vibration.

- **Mounting Strategy**

Boundary conditions imposed by the chassis determine how vibration energy is transferred to the PCB. Rigid four-corner mounting provides higher modal frequencies but increases stress gradients around the fasteners. Adding intermediate standoffs, compliant mounts, or damping layers can redistribute deformation and reduce solder-joint strain energy. Proper mounting selection is therefore one of the most effective design measures for enhancing vibration reliability**.**

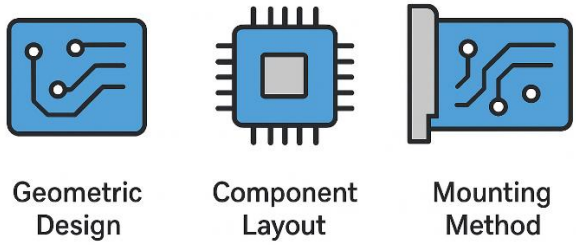

Figure 3. Design and Structural Factors Affecting the Lifetime of an Electronic Board

2.4.2 Environmental Conditions

Environmental stressors modulate the fatigue behavior of solder joints by altering dynamic response, material properties, or crack-propagation mechanisms. Key environmental factors are presented in Figure 4.

- **Vibration Intensity and Amplitude**

The severity of random vibration, typically characterized by power spectral density (PSD) and root mean square (RMS) acceleration, directly influences PCB deflection and solder joint strain. Elevated PSD levels, particularly those exceeding 5 g RMS as commonly observed in aerospace applications, increase stress amplitudes and significantly reduce fatigue life. The integration of vibration isolators or damping structures can mitigate the effective stress environment, leading to fatigue life improvements of up to 40%.

- **Temperature**

Temperature affects solder alloy stiffness, creep rate, and intermetallic growth. Elevated temperatures accelerate time-dependent viscoplastic deformation, while thermal cycling introduces CTE-mismatch stresses between component packages and the PCB substrate. The use of high-Tg laminates, thermal vias, and optimized heat-spreading materials helps stabilize mechanical properties and extend fatigue life.

- **Humidity**

High humidity promotes oxidation, corrosion, and microcrack nucleation in solder joints and copper traces. Moisture absorption also reduces the mechanical stiffness

of polymeric substrates. Applying conformal coatings (e.g., acrylic, polyurethane) mitigates these effects by providing moisture barriers and stabilizing interfacial behavior.

- **Mechanical Shock**

Transient shocks during handling, transport, or mission events can impose large instantaneous stresses that, when combined with random vibration, significantly accelerate fatigue damage. Compliance with shock-qualification standards is therefore critical for systems deployed in aerospace and defense environments.

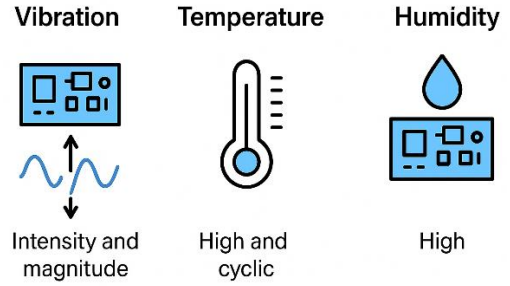

Figure 4. Environmental Conditions Factors Affecting the Lifetime of the Electronic Board

2.4.3 Material Properties

The choice of materials used in solder alloys, PCB substrates, and protective coatings has a decisive influence on fatigue performance under random vibration. Material behavior under thermal, mechanical, and environmental loading must therefore be carefully considered to ensure long-term reliability.

- **Solder Alloys**

Solder joints represent the most common failure sites in PCBs exposed to random vibration. Lead-free solders, such as SAC305 (Sn-Ag-Cu), generally exhibit good fatigue resistance at lower temperatures but are prone to creep under elevated conditions. In contrast, traditional lead-based solders demonstrate superior fatigue endurance but are largely restricted due to environmental regulations such as RoHS. Optimized solder alloy selection, tailored to the operational thermal and vibration environment, can improve fatigue life by up to 50%.

- **PCB Substrate Materials**

The mechanical and thermal properties of the substrate strongly affect vibration response and solder joint reliability. FR4, the most widely used PCB material, offers acceptable performance in standard applications but softens at temperatures above approximately 130 °C, reducing structural stiffness. Alternative materials such as polyimide laminates (resistant up to ~260 °C) or ceramic substrates provide significantly higher stability under combined thermal and vibrational loads, making them suitable for aerospace, automotive, and other high-reliability sectors.

- **Protective Coatings**

Conformal coatings and encapsulants play an essential role in mitigating environmental degradation and reducing vibrational stress. Polyurethane coatings are effective in protecting against moisture and mild vibration, while epoxy-based coatings are more suitable for high-temperature conditions. By preventing oxidation and redistributing vibrational energy, appropriate protective coatings can extend PCB service life by 30-50%, particularly in humid or high-vibration environments. Figure 5 shows the material property factors influencing the lifetime of the electronic board.

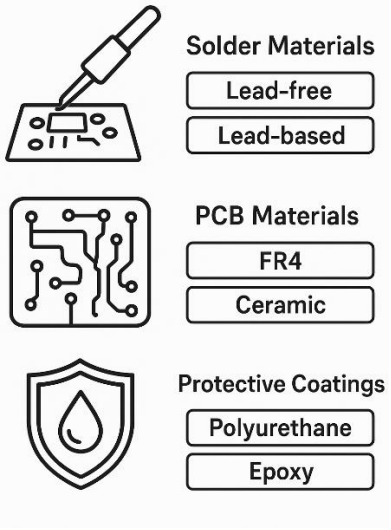

Figure 5. Material Properties Factors Affecting the Lifetime of the Electronic Board

2.5 Damage Mechanisms in Solder under Vibrations Loading

The accumulation of damage in high-stress regions and subsequent crack propagation governs fatigue mechanisms in solder joints. These processes are strongly influenced by factors such as natural frequency, solder alloy properties, and operating temperature. The dominant damage mechanisms include:

1. **Cyclic Stress Induced Cracking:** Random vibrations generate cyclic stresses within solder joints, particularly at stress concentration sites such as joint edges or solder balls. The accumulation of strain energy initiates microcracks, which propagate under repeated loading cycles until the final fracture occurs. This progressive transition from elastic to plastic deformation is commonly modeled using the Coffin–Manson and Paris fatigue models.
2. **Dynamic Creep under Vibrational Loading:** At elevated temperatures, continuous dynamic loading from random vibrations can induce creep in solder alloys. This time-dependent permanent deformation arises from mechanisms such as grain boundary sliding and atomic diffusion. Predictive approaches, including the Anand and Norton–Bailey models, are widely used to capture creep behavior in solders.
3. **Resonance Induced Fatigue**: When the excitation spectrum overlaps with the natural frequency

of the PCB or component, resonance occurs. This dramatically amplifies vibration amplitudes and stress levels, accelerating failure. Stress concentrations are particularly severe in electronic packages such as BGAs (ball grid arrays), often beneath the die region. Modal and harmonic analyses using finite element methods (e.g., ANSYS) are essential for identifying resonance conditions.

4. **Transverse Vibration Induced Damage**: Transverse vibrations cause board bending, which transfers lateral forces to solder joints. These forces lead to tensile stress accumulation and crack initiation, particularly in joints near the board edges.

5. **Thermo Mechanical Stresses under Combined Loading**: Mismatch in the coefficient of thermal expansion (CTE) between solder and PCB materials induces alternating tensile and compressive stresses, especially at high operating temperatures. When coupled with random vibration, these stresses accelerate crack growth and internal damage within solder joints.

6. **Oxidation and Chemical Degradation**: Moist or contaminated environments promote oxidation and the formation of weak intermetallic layers at solder surfaces. These layers reduce the mechanical strength of the joints and encourage secondary crack formation, further compromising reliability. Based on these mechanisms, solder-related failures in PCBs subjected to random vibration can generally be classified into two categories:

- Failures occurring in solder joints of electronic components (Figure 6A)
- Failures occurring in component leads or terminations (Figure 6 B)

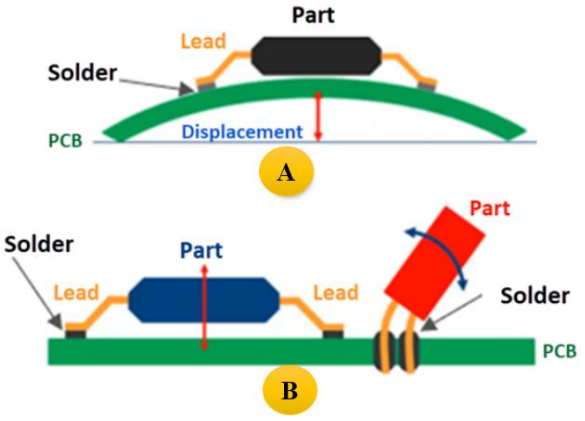

Figure 6. Mechanism of Fracture in Solder Joint

In conclusion, the theoretical foundations presented in this chapter establish the analytical framework for interpreting vibration-induced fatigue in electronic assemblies. These foundations encompass PSD-based random vibration analysis, sinusoidal resonance evaluation, frequency-domain fatigue modeling, and Weibull-based probabilistic life estimation. Collectively, they provide the essential basis for linking vibrational loading to fatigue failure through quantifiable mechanical and statistical indicators.

Building upon these theoretical elements, Chapter 3 applies them within a finite element modeling environment to predict the dynamic response of multilayer PCBs populated with BGA, LCCC, and leaded components. This implementation integrates modal analysis, harmonic response evaluation, and stress extraction procedures to generate the physics-based inputs required for subsequent fatigue life and reliability assessment.

3. Methodology for Finite Element Modeling and Vibration Fatigue Analysis of Solder Joints

The analysis of electronic packages under random vibration loading is critical for predicting reliability and lifetime in demanding applications such as aerospace, automotive, and military environments. Packages like Ball Grid Array (BGA), Quad Flat Package (QFP), Leadless Ceramic Chip Carrier (LCCC), Chip Scale Package (CSP), and leaded configurations (e.g., Dual In-line Package (DIP) and Small Outline Integrated Circuit (SOIC)) exhibit distinct behaviors due to differences in design, materials, and interconnect structures. Understanding stress and damage mechanisms under random vibrations guides design optimization and failure mitigation.

Random vibrations, characterized by broadband frequency spectra (typically 20–2000 Hz) and power spectral density (PSD) profiles, simulate real-world operational conditions and can lead to high-cycle fatigue failures in solder joints or leads. Predictive models, such as Steinberg's three-band technique and Miner's cumulative damage rule, estimate lifetime by accounting for stress accumulation and Gaussian response distributions. Finite element analysis (FEA) and experimental testing validate these predictions, considering factors like lead-free (Pb-free) vs. leaded solders, which influence creep and fatigue resistance.

1. Ball Grid Array (BGA) Configuration

BGA packages feature a uniform array of solder balls, offering compact size and high pin counts for aerospace and automotive applications. Under random vibration, stress concentration occurs primarily in the outer or corner solder balls due to relative displacement between the package and the printed circuit board (PCB), rather than at the center. Regions like the "die shadow" (beneath the silicon die) and peripheral areas experience elevated shear and tensile stresses, exacerbated by resonance near natural frequencies. Pb-free solders (e.g., SAC alloys) show increased vulnerability compared to Sn-Pb, with lifetime predictions based on Basquin's high-cycle fatigue model integrated with Miner's rule. Optimization strategies, such as underfill materials or structural stiffeners, reduce equivalent von Mises stress. Figure 7

illustrates a schematic of the die shadow in a BGA package.

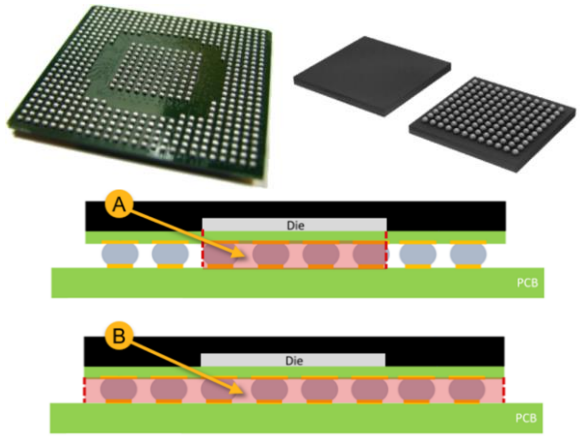

Figure 7. Schematic of Die Shadow in BGA Package

2. Quad Flat Package (QFP) Configuration

QFP packages utilize gull-wing or flat leads, making corner leads susceptible to tensile and shear stresses under random vibration. Extended lead length amplifies bending moments, leading to fatigue failures at the lead–solder interface or package corners. Experimental studies indicate that solder fatigue dominates over lead fracture, with lifetime assessments using Taguchi methods or three-band techniques for PSD-based predictions. In automotive environments, combined vibration and thermal cycling accelerate degradation, necessitating robust design modifications such as lead forming or damping materials. Figure 8 presents a schematic of the QFP package.

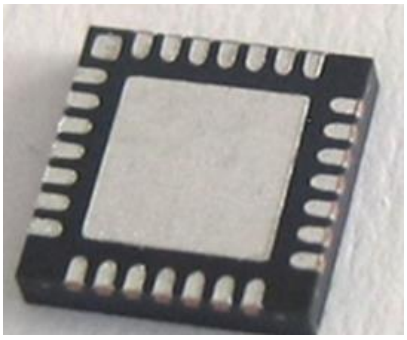

Figure 8. Schematic of QFP Package

3. Leadless Ceramic Chip Carrier (LCCC) Configuration

LCCC packages, with ceramic substrates and castellation interconnects, are suited for high-temperature and vibration-prone military and industrial applications due to their thermal stability and rigidity. Random vibrations induce compressive and tensile stresses at the ceramic solder interface, potentially causing microcracks or delamination. Reliability is enhanced by high melting point solders, with fatigue life improved through optimized solder joint height and compliance with MIL-STD-810. Simulations show that harsh environments reduce lifetime, but ceramic's low CTE mismatch with PCBs mitigates risks. Figure 9 shows a schematic of the LCCC package.

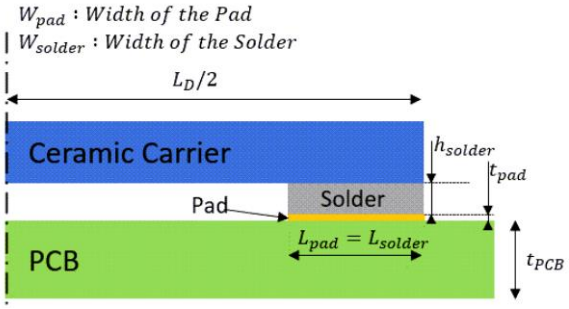

Figure 9. Schematic of LCCC Package

4. Leaded Package Configuration

Leaded packages, such as DIP and SOIC, incorporate flexible metal leads that absorb mechanical shocks and vibrations, making them suitable for industrial and military uses. Elongated leads distribute shear and bending stresses, reducing PCB damage but increasing vulnerability at lead–PCB joints. Failures occur due to frequency-dependent amplitude variations, with reliability testing per MIL-STD-883 emphasizing vibration isolation or stiffeners. Pb-free variants exhibit altered fatigue behavior, necessitating probabilistic models for lifetime estimation in aerospace deployments. Figure 10 illustrates a schematic of the leaded package.

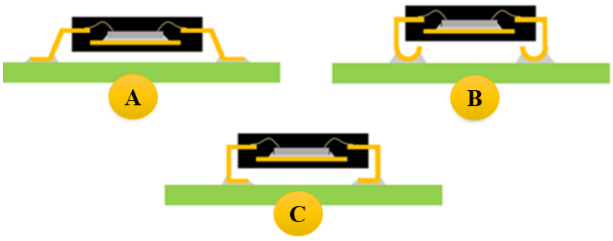

Figure 10. Schematic of Leaded Package

3.1 Finite Element Modelling of a Multilayer Electronic Circuit Board

Finite element modeling (FEM) was conducted to evaluate the dynamic response and fatigue-critical stress fields of a multilayer printed circuit board (PCB) subjected to random vibration loading. The PCB comprises 189 electronic components, including resistors, capacitors, transistors, and integrated circuits arranged in a high-density configuration representative of aerospace and defense-grade hardware. Its multilayer structure consists of six copper layers (0.5–1 oz; 17.5–35 μm) separated by five FR-4 dielectric laminates.

The FR-4 dielectric material was modeled as an orthotropic elastic medium (E ≈ 27 GPa, ν = 0.28, Tg ≈ 135 °C, CTE ≈ 16 ppm/°C), while the copper layers were treated as isotropic elastic solids (E ≈ 110 GPa, ν = 0.34).

All large components, such as BGAs, LCCCs, and leaded IC packages, were included with full geometric fidelity. Small passive components were simplified to reduce computational cost while maintaining equivalent mass and stiffness distribution.

A multi-resolution meshing strategy was employed using a hybrid combination of hexahedral and tetrahedral elements to capture both planar PCB regions and complex component geometries accurately. The global element size of 5 mm was locally refined to 0.5 mm in areas of high component density and around solder joint interfaces, resulting in approximately 70,000 elements in the final mesh. To ensure solution accuracy, a mesh convergence study was performed, refining the model from 20,000 to 120,000 elements over 12 refinement levels. The first three natural frequencies, approximately 181 Hz, 382 Hz, and 490 Hz, converged with less than 2% variation beyond 70,000 elements, confirming adequate mesh resolution. As expected, modal frequencies decreased with refinement, reflecting improved stiffness representation, particularly near component-rich regions where local curvature strongly affects bending modes.

The PCB was constrained at mounting-hole locations to replicate the chassis installation conditions typical of aerospace systems. Random vibration loading was applied via a base-excitation power spectral density (PSD) profile spanning 20–2000 Hz, consistent with MIL-STD-810 and NASA GEVS standards. Modal analysis was performed to extract natural frequencies and mode shapes, identifying the first out-of-plane bending mode at 181 Hz as the dominant contributor to vibration-induced solder fatigue. Subsequently, harmonic response analysis was conducted to evaluate resonant amplification and peak von Mises stress distributions near critical interconnect regions.

Random vibration analysis was then carried out using the PSD input to compute RMS stresses, displacements, and accelerations across the PCB. These results provided the stress amplitude distributions necessary for fatigue life estimation via Miner's rule, and probabilistic life prediction via Weibull modeling. To resolve steep stress gradients near critical packages, particularly BGA components, submodeling techniques were employed. Localized, highly refined submodels incorporating contact elements at component–PCB interfaces were developed to capture shear and tensile stresses transmitted into solder joints under dynamic loading. This strategy enabled accurate resolution of local stress concentrations that could not be captured by the global model alone.

Overall, the FEM workflow comprising multilayer structural representation, hybrid meshing, mesh convergence validation, modal extraction, harmonic analysis, and PSD-based random vibration response establishes a physics-informed foundation for fatigue and reliability assessment. This integrated modeling framework ensures that both global board-level dynamics and localized solder-joint behavior are represented with sufficient fidelity to support high-confidence predictions of vibration-induced fatigue in aerospace-grade electronic assemblies. Figure 11 depicts a schematic of the meshed multilayer PCB.

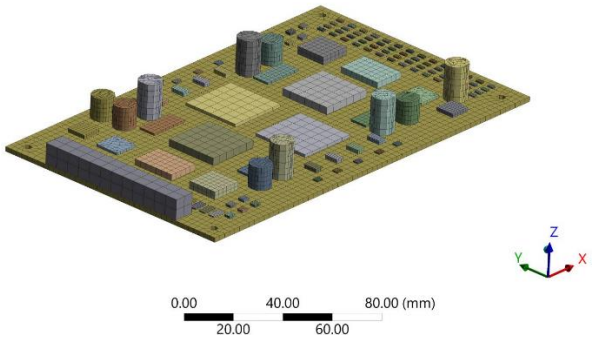

Figure 11. Schematic of the meshed multilayer PCB

Figure 12 shows the mesh independence study of modal frequencies as a function of the number of elements.

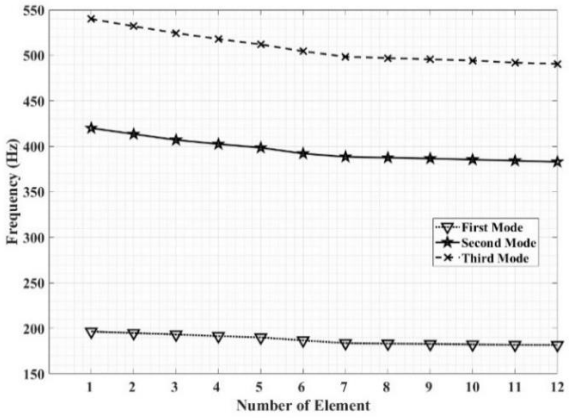

Figure 12. Mesh independence study of modal frequencies versus number of elements

Following the mesh independence study, the analysis proceeds to visualizing the first three modal shapes of the PCB, as shown in Figures 13, 14, and 15. These figures illustrate the deformation patterns corresponding to the converged natural frequencies of approximately 181 Hz, 382 Hz, and 490 Hz, respectively. The first mode demonstrates out-of-plane bending, while the second and third modes reveal torsional and higher-order bending responses. These visualizations, obtained from ANSYS modal analysis, provide critical insights into potential stress concentrations, supporting design optimization and the reliability assessment of the PCB under random vibration loading.

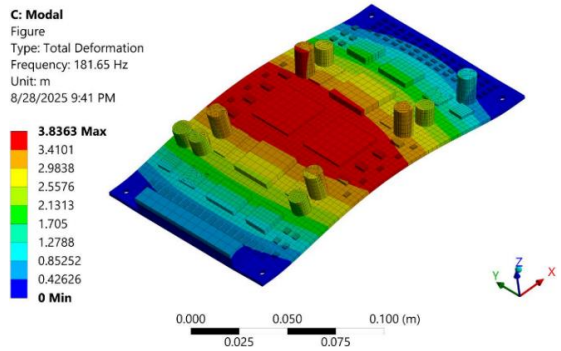

Figure 13. First Mode Shape of PCB

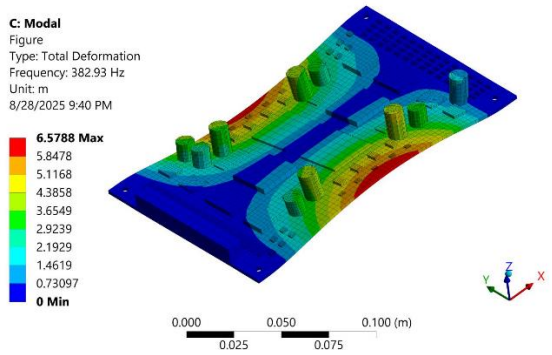

Figure 14. Second Mode Shape of PCB

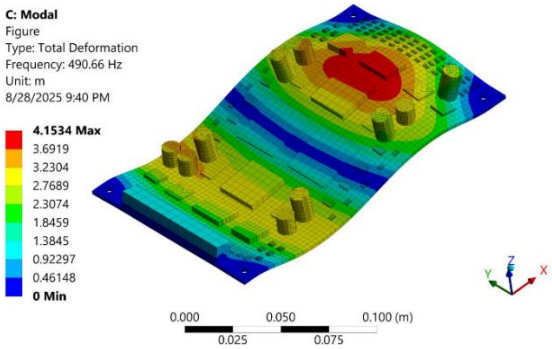

Figure 15. Third Mode Shape of PCB

3.2 Vibration Loading Profile

To simulate random vibration conditions, a power spectral density (PSD) profile defines the distribution of vibrational energy across specified frequency bands. The profile spans a frequency range from 20 Hz to 2000 Hz, with a plateau of 0.1 (g^2/Hz) between 200 Hz and 2000 Hz, representing typical operational environments. The root mean square (RMS) acceleration is set at 14.72 Grms, reflecting the effective vibration amplitude. This PSD input (Figure 16), applied in the ANSYS random vibration analysis, enables the evaluation of fatigue life and stress distribution across the PCB's 189 components, ensuring consistency with real-world dynamic loading conditions.

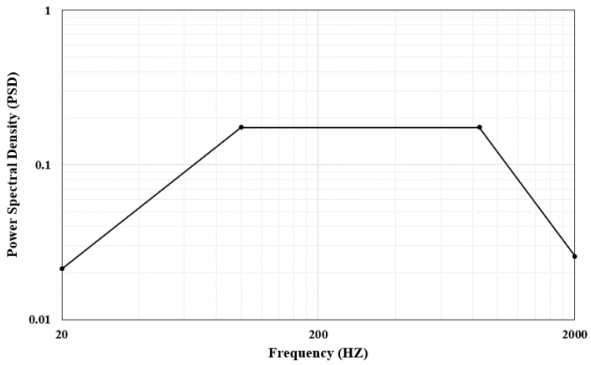

Figure 16. Power Spectral Density (PSD) profile for random vibration analysis

To evaluate the PCB's response under flight-level sinusoidal vibration, loading profiles are defined for both axial and lateral directions, as illustrated in Figures 17 and 18, respectively. Figure 17 presents the axial vibration profile, characterized by a sinusoidal acceleration input that varies with frequency to simulate longitudinal flight-induced stresses. Figure 18 depicts the lateral vibration profile, representing transverse dynamic loads experienced during flight. These profiles, applied using the ANSYS harmonic analysis module, cover a frequency range of 10–100 Hz, with peak acceleration values tailored to actual flight conditions. This approach enables a comprehensive assessment of the reliability of the PCB's 189 components under directional sinusoidal excitation.

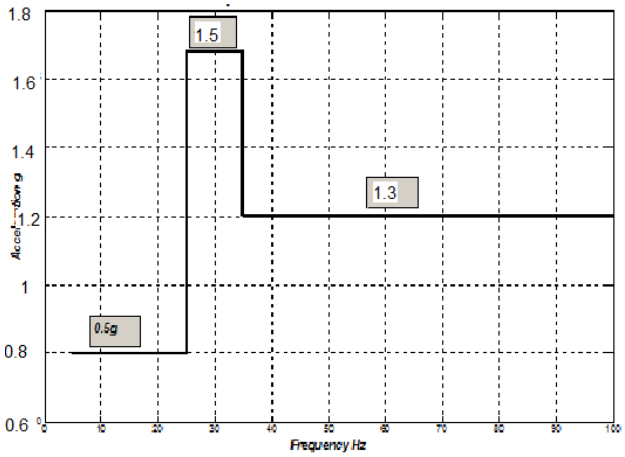

Figure 17. Sinusoidal vibration loading profile for axial direction

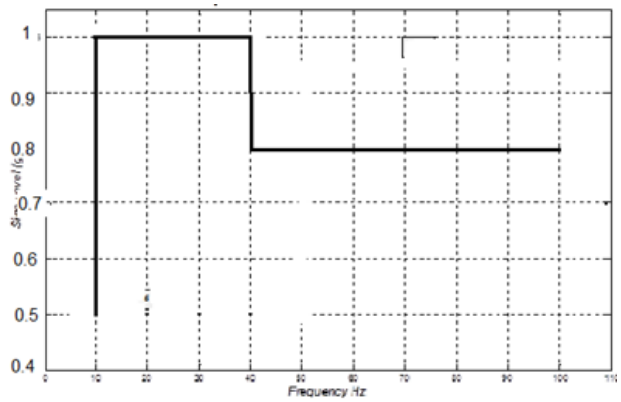

Figure 18. Sinusoidal vibration loading profile for the Lateral direction

4. Results and Discussion

The numerical simulations and subsequent analyses offer a comprehensive understanding of vibration-induced fatigue behavior in solder joints across various package configurations. The results are presented systematically to highlight the influence of loading conditions, geometric variations, and material properties on stress distribution, strain localization, and fatigue life.

This chapter discusses the outcomes of the finite element analysis (FEA) in a structured manner. Initially,

the global response of the models, such as displacement fields and natural frequency extraction, is presented to validate the accuracy of the developed simulation framework. This is followed by detailed contour plots of stress and strain distributions, which identify critical regions with high stress concentration factors (Kt). Comparative assessments are carried out for BGA, LCCC, and leaded packages under different vibration scenarios, including single-axis and multi-axis excitations at varying acceleration levels.

Fatigue life predictions are further evaluated using Weibull distribution fitting, yielding key reliability metrics such as the shape parameter (β), scale parameter (η), mean time to failure (MTTF), and B10 life. Sensitivity analyses are also performed to assess the impact of mesh density and geometric variables, such as solder ball diameter in BGAs, lead dimensions in leaded packages, and pad spacing in LCCCs, on overall fatigue performance.

The discussion not only interprets numerical results but also explores their practical implications for aerospace electronic packaging design. Findings are contextualized with existing experimental data and theoretical models, highlighting the capabilities and limitations of the proposed methodology while outlining recommendations for future research.

4.1 Response of the Electronic Board under Sinusoidal and Random Vibration Loading

To accurately capture the dynamic behavior of electronic boards under aerospace vibration conditions, frequency response analyses were conducted using both sinusoidal and random excitation profiles. Sinusoidal excitation offers insights into resonance phenomena, mode shapes, and the amplification of displacement and stress near natural frequencies. In contrast, random vibration loading, which more closely replicates launch and in-orbit operational environments, allows evaluation of the statistical distribution of stress and strain energy across solder joints.

The results are presented in two parts. First, the sinusoidal sweep analysis illustrates displacement and stress amplitude as functions of excitation frequency, highlighting critical resonance peaks for each package type (BGA, LCCC, Leaded). Modal frequencies are extracted and correlated with finite element predictions to validate the numerical model. Second, random vibration analyses are performed using power spectral density (PSD) input profiles. The resulting output responses, including root mean square (RMS) displacements, stresses, and strain energy densities, are compared across package configurations to identify critical failure-prone regions.

These results provide the foundation for subsequent fatigue life estimations and statistical reliability analyses presented in later sections. They also demonstrate the significant differences in vibration response between sinusoidal and random loading, underlining the importance of considering both excitation types in aerospace reliability assessments.

The finite element analysis of the multilayer printed circuit board (PCB) under random and sinusoidal vibration loading reveals distinct stress distributions, as shown in Figures 19 and 20, respectively. Figure 19 presents the equivalent (von Mises) stress distribution resulting from random vibration analysis, conducted with a 1-sigma scale factor and a peak stress of 223.52 MPa. This analysis, based on a PSD profile with an RMS acceleration of 14.72 Grms, highlights broad stress concentrations across the PCB, particularly at component interfaces and solder joints, with a probability of 68.269%. The maximum stress of 223.52 MPa indicates significant dynamic loading effects, reflecting the cumulative impact of broadband frequencies (20–2000 Hz) on the 189 components.

In contrast, Figure 20 depicts the equivalent stress distribution from a harmonic response analysis at 100 Hz, with a peak stress of 8.4007 MPa. This sinusoidal loading, applied with a zero-degree phase sweep, produces a more localized stress pattern, with peak values concentrated around specific components such as the central IC chip and cylindrical elements. The lower peak stress (8.4007 MPa), compared to the random vibration case, underscores the narrower frequency range (100 Hz), which excites resonant modes less intensively than the random broadband input.

The comparative analysis shows that random vibration induces higher overall stress levels due to its wide frequency spectrum, potentially accelerating fatigue failure in solder joints as evidenced by the 223.52 MPa maximum. Sinusoidal vibration, however, generates localized stress peaks, suggesting a resonance risk at specific frequencies, though with a lower magnitude (8.4007 MPa). The broader impact of random vibration aligns with real-world flight conditions, while the sinusoidal case effectively isolates modal responses.

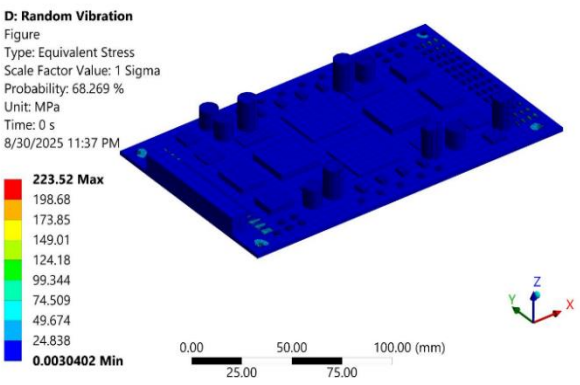

Figure 19. Equivalent stress distribution under random Vibration

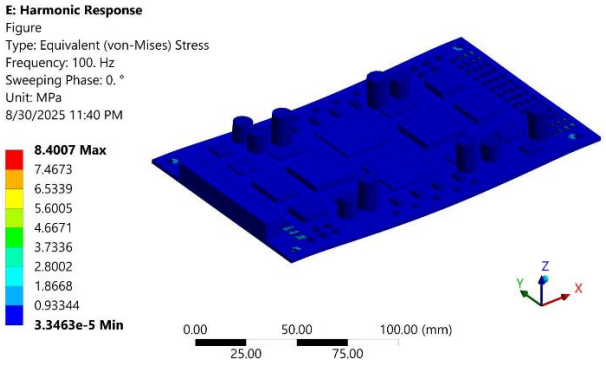

Figure 20. Equivalent stress distribution under sinusoidal vibration

The analysis evaluates the deformation of the printed circuit board (PCB) under random and sinusoidal vibration loading, as shown in Figures 21 and 22, respectively. Figure 21 illustrates the directional deformation along the Z-axis under random vibration, with a maximum displacement of 0.47217 mm at a 1-sigma scale factor (68.269% probability). This broad deformation pattern, driven by a power spectral density (PSD) profile ranging from 20 to 2000 Hz with an RMS acceleration of 14.72 Grms, reflects the cumulative effect of broadband frequencies. Significant displacement is observed around the central IC chip and cylindrical components.

In contrast, Figure 22 depicts the total deformation under sinusoidal loading at 100 Hz, with a peak displacement of 0.057206 mm. The harmonic response analysis, using a zero-degree phase sweep, reveals a more localized deformation, peaking at the central region and diminishing toward the edges. The lower maximum deformation under sinusoidal loading (0.057206 mm), compared to that under random vibration (0.47217 mm), highlights the narrower frequency range, which excites specific resonant modes less intensely.

This comparison indicates that random vibration induces greater overall deformation due to its broad frequency spectrum, posing a higher risk of fatigue in solder joints. Sinusoidal loading, however, produces concentrated deformation at resonant frequencies, suggesting potential localized failure risks.

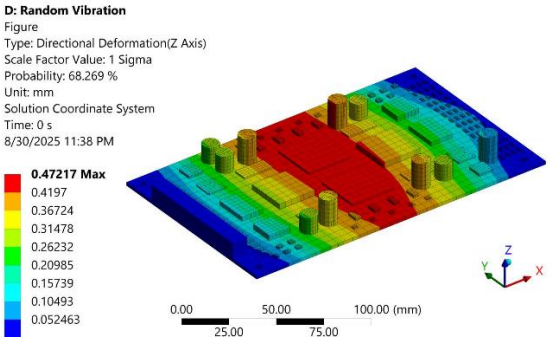

Figure 21. Directional deformation (Z axis) under random vibration

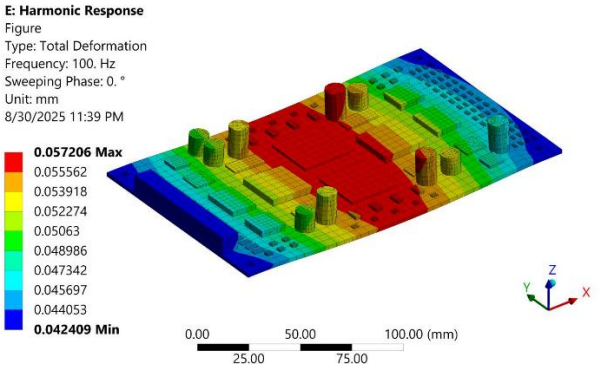

Figure 22. Total deformation under sinusoidal vibration

4.2 Frequency Response Analysis of Electronic Packages under Random Vibration Loading

The finite element analysis (FEA) of electronic packages under random vibration loading provides critical insights into their dynamic behavior and reliability, particularly in high-vibration environments such as aerospace and automotive applications. In this study, a random vibration load with a root mean square (RMS) acceleration of 14.72 Grms was applied to a multilayer printed circuit board (PCB) hosting Ball Grid Array (BGA), Leadless Ceramic Chip Carrier (LCCC), and Leaded packages. The power spectral density (PSD) profile spanned 20–2000 Hz, simulating broadband operational conditions. Frequency response functions (FRFs) for each package, derived from ANSYS simulations, illustrate the response acceleration (in g^2/Hz) versus frequency, enabling the evaluation of resonance peaks, stress amplification, and fatigue life prediction using models such as Steinberg's three-band technique and Miner's cumulative damage rule.

The FRFs for the three packages exhibit distinct patterns, reflecting their structural designs. For the BGA package, the response features a prominent initial peak at approximately 100 Hz, reaching +30 g^2/Hz, followed by subsequent oscillations with negative amplitudes down to −20 g^2/Hz. This pronounced resonance indicates high relative displacement between the package and the PCB, concentrating shear and tensile stresses in the outer solder balls, which exacerbates high-cycle fatigue. In contrast, the LCCC FRF shows a slightly attenuated initial peak (+20 g^2/Hz) but stronger negative oscillations (−30 g^2/Hz) at higher frequencies. This is attributed to the ceramic substrate's rigidity, which distributes stresses more evenly but increases the risk of microcracking at solder interfaces due to direct vibration transmission. The Leaded package FRF mirrors the LCCC in peak magnitude (+20 to −30 g^2/Hz). Still, it displays smoother oscillations, owing to the compliant leads that act as dampers, absorbing bending and shear stresses and reducing transmission to solder joints.

These differences stem primarily from interconnect architectures: BGA's leadless solder balls facilitate direct stress transfer, amplifying resonance; LCCC's ceramic rigidity offers thermal stability but limited mechanical compliance; and Leaded packages, with flexible leads, provide mechanical isolation, mitigating peak responses. Under the applied 14.72 Grms load, the BGA exhibits the highest response amplitudes, leading to accelerated fatigue, while the Leaded package shows the lowest effective stress amplification.

Lifetime predictions, based on FRF-derived RMS stresses and JEDEC/MIL-STD standards, rank the packages as follows: Leaded > LCCC > BGA. Leaded packages demonstrate superior durability due to their vibration-damping capabilities, making them preferable for vibration-prone applications, whereas BGAs require enhancements such as underfills to achieve comparable reliability. Future work should incorporate experimental validation to refine these numerical models. Figures 23–25 present the frequency response functions (FRFs) of the BGA, LCCC, and leaded packages under random vibration.

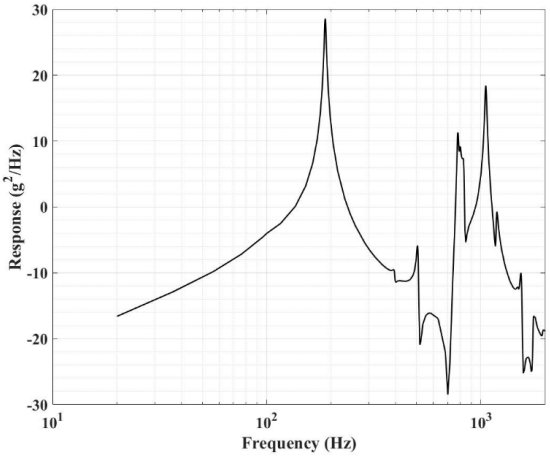

Figure 23. Frequency Response Function (FRF) of the BGA package under random vibration

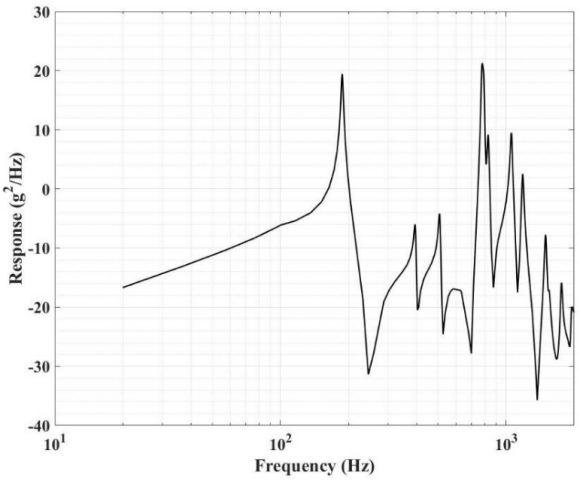

Figure 24. Frequency Response Function (FRF) of the LCCC package under random vibration

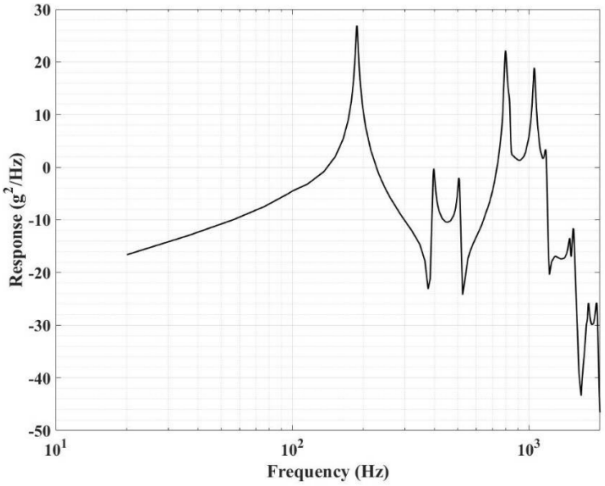

Figure 25. Frequency Response Function (FRF) of the Leaded package under random vibration

4.3 Comparative Evaluation of Stress and Deformation under Uniaxial and Triaxial Vibration Loading

This study presents a comparative finite element analysis (FEA) of stress and deformation distributions within a multilayer printed circuit board (PCB) subjected to uniaxial and triaxial vibration loading, utilizing ANSYS Workbench. The motivation stems from the growing recognition that multiaxial vibration, such as that experienced during spacecraft launch, induces more severe fatigue degradation in solder interconnects than conventional uniaxial tests. However, most qualification standards remain based on single-axis methodologies.

The PCB under investigation contained 189 electronic components, including ball grid arrays (BGAs), leadless ceramic chip carriers (LCCCs), and conventional leaded packages. A three-dimensional CAD-based geometry was imported into ANSYS, and a hybrid meshing scheme was employed, using hexahedral elements in regions of uniform stress and localized tetrahedral refinement in solder joints to capture stress gradients accurately.

Material properties for the FR4 substrate, copper traces, and SAC305 solder alloy were assigned, with elastic modulus, Poisson's ratio, and density calibrated against IPC-7095 guidelines. Boundary conditions assumed rigid clamping along one PCB edge, consistent with board-level vibration test fixtures.

Two classes of vibrational loading were considered. The random vibration excitation followed a power spectral density (PSD) profile spanning 20–2000 Hz with a root mean square (RMS) acceleration of 14.72 Grms. The sinusoidal case involved a swept-sine excitation in the out-of-plane direction at 100 Hz, with amplitude scaling based on Figures 16 and 17.

The stress contour results demonstrated pronounced differences between loading scenarios. Under triaxial vibration loading (Figure 26), the maximum von Mises

stress reached 387.15 MPa, compared to 223.52 MPa under the uniaxial counterpart (Figure 19). Stress localization occurred predominantly at the corner solder joints of BGA packages and at intermetallic compound (IMC) layers at the component–PCB interface, consistent with previously reported failure sites.

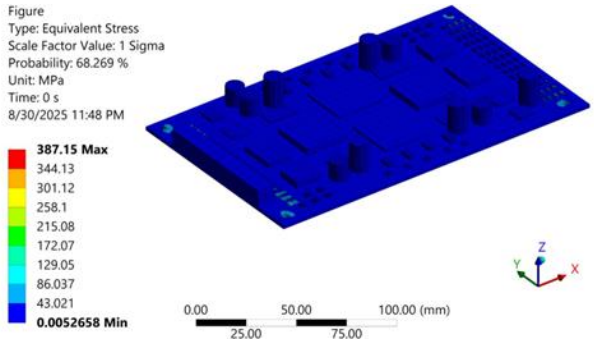

Figure 26. Equivalent stress distribution under Tri Axial Vibration Loading

4.4 Comparative Reliability Assessment of BGA, Leaded, and LCCC Packages under Vibration-Induced Fatigue

The comparative analysis of probability-of-failure versus life diagrams for Ball Grid Array (BGA), Leaded, and Leadless Ceramic Chip Carrier (LCCC) packages provides critical insight into their respective vibration fatigue reliability. Such probability plots, derived from Weibull cumulative distributions, offer not only estimates of mean time to failure but also characterize the statistical spread of early and late-life failures. This enables rigorous evaluation of packaging architectures under vibration-dominated loading conditions, a factor of paramount importance in aerospace electronics, where repair is infeasible, and reliability margins must be maximized.

The BGA package exhibits the least favorable reliability characteristics among the three designs. Its probability-of-failure curve shows an early onset of failures, with the 10% probability threshold reached at relatively low cycle counts. Furthermore, the steep gradient of the curve indicates a narrow scatter of lifetimes, suggesting that once fatigue initiation occurs, failure progression accelerates across multiple solder joints. This behavior stems from the intrinsic geometry of BGAs: spherical solder balls with limited compliance, serving as the primary load-bearing interconnects. Under multiaxial vibration, the peripheral joints, particularly at the corners, experience amplified shear and tensile strains due to board bending modes and coefficient of thermal expansion (CTE) mismatch. The lack of compliant leads results in direct transmission of vibrational energy into the solder–substrate interface, accelerating crack nucleation within the intermetallic compound (IMC) layer. Consequently, despite their high I/O density and functional advantages, BGAs represent the least reliable configuration under vibration-induced fatigue loading.

In contrast, the leaded package demonstrates the most robust fatigue resistance. Its probability-of-failure curve shifts significantly toward longer lifetimes, with a delayed onset of initial failures. Moreover, the curve's slope is comparatively shallow, reflecting a broader scatter and the presence of samples capable of sustaining substantially longer operational durations. This superior reliability is attributable to the mechanical compliance of the metallic leads, which act as effective stress-relief elements. By decoupling the solder joints from direct vibrational loading, the leads reduce localized strain accumulation, thereby lowering the likelihood of crack initiation. Even when damage begins to develop, the energy-dissipating nature of the leads moderates crack growth rates, extending the effective fatigue life of the package. While manufacturing variability or voiding may still induce occasional early-life failures, the overall lifetime distribution clearly demonstrates that leaded assemblies possess the highest inherent tolerance to vibration fatigue.

The LCCC package occupies an intermediate reliability domain between BGA and leaded designs. Its probability curve indicates an improvement over BGA, with delayed failure onset and a somewhat higher characteristic life. However, the slope of the curve remains relatively steep, signifying reduced tolerance once fatigue cracks initiate. The rigid ceramic housing of the LCCC contributes to dimensional stability but simultaneously imposes severe constraints on strain accommodation. Without the benefit of compliant leads, solder pads are forced to absorb most of the vibrational deformation. As a result, localized stress concentrations form at the solder–ceramic interface, where brittle fracture modes dominate once fatigue begins. Compared to BGAs, the planar pad attachment provides a stronger initial metallurgical bond, which explains the delay in failure onset. Nevertheless, in terms of lifetime extension and resistance to high-cycle fatigue, LCCCs remain inferior to leaded configurations.

Taken collectively, the comparative diagrams establish a clear hierarchy of fatigue resistance under vibration: leaded packages demonstrate the longest operational lifetimes, LCCCs provide intermediate performance, and BGAs exhibit the shortest. This outcome underscores the critical role of package compliance in mitigating vibration-induced strains at the solder joint level. The mechanical buffering afforded by leads provides a decisive advantage in environments characterized by broadband and multiaxial loading. While the trend toward high-density integration necessitates the use of BGAs and LCCCs, their adoption requires supplementary mitigation measures such as underfill encapsulation, corner staking, or PCB stiffeners to approach the reliability margins inherently offered by leaded designs. Ultimately, the probability-of-failure versus life analysis validates that

packaging architecture remains the dominant factor dictating solder joint survivability under vibration fatigue. Figures 27–29 show the lifetime of the BGA, LCCC, and leaded packages, respectively.

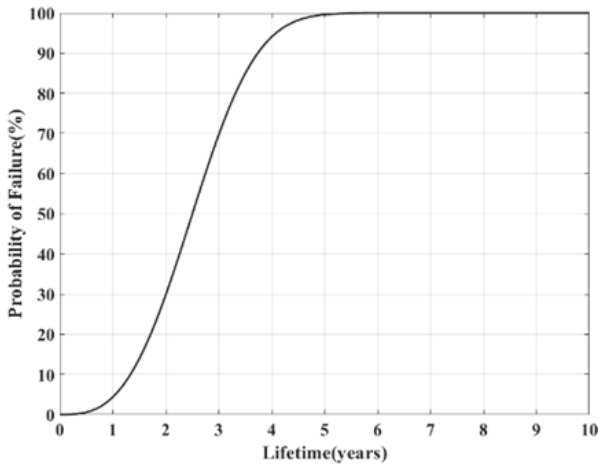

Figure 27. BGA Package Life Time

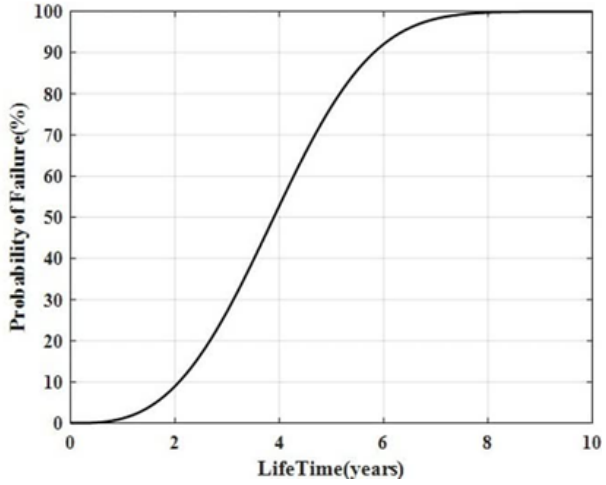

Figure 28. LCCC Package Life Time

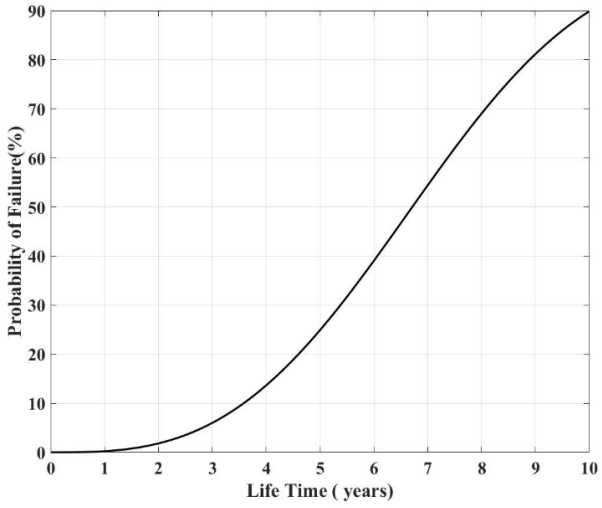

Figure 29. Leaded Package Life Time

4.5 Influence of Solder Alloy Composition on the Reliability of BGA Packages under Vibration Loading

The reliability of solder interconnects in electronic assemblies is strongly influenced by the intrinsic properties of the solder alloy. Mechanical robustness, ductility, creep resistance, and fracture toughness all play significant roles in determining how long a solder joint can endure cyclic thermomechanical or vibration-induced loads before fatigue failure initiates and propagates. To demonstrate the critical role of alloy selection in solder joint reliability, a case study was performed using a Ball Grid Array (BGA) package subjected to vibration loading. The analysis compares three widely utilized alloys, SAC305 (Sn96.5Ag3Cu0.5), PB90SN10 (Pb90Sn10), and SN100C (SnCu0.7NiGe), and evaluates their relative fatigue lifetimes in terms of probability of failure versus time. The results, presented in Figure 28, clearly illustrate the marked differences in reliability performance across these solder compositions.

Among the three materials, PB90SN10 exhibits the weakest durability under vibration-induced fatigue. Its probability of failure curve rises steeply within the first few years, reaching nearly complete failure in less than three years. This rapid degradation can be attributed to the metallurgical and mechanical characteristics of high-lead solders. While traditionally employed in high-reliability aerospace systems for their creep resistance at elevated temperatures, Pb-rich alloys often exhibit poor vibration fatigue performance due to their relatively low ductility and susceptibility to early crack initiation under dynamic cyclic loading. In this case, the steep slope of the PB90SN10 curve reflects its limited ability to absorb vibrational strain energy without undergoing localized plastic deformation and subsequent crack propagation. As a result, PB90SN10 appears unsuitable for vibration-dominated environments where solder joints are repeatedly subjected to multiaxial excitation over extended mission lifetimes.

The SN100C alloy demonstrates a more balanced performance. Its probability of failure curve increases at a slower rate compared to PB90SN10, suggesting an improved ability to withstand vibrational stresses during the mid-lifetime window of operation. The addition of small amounts of nickel and germanium to the Sn–Cu system is known to refine the intermetallic microstructure, suppress excessive Cu–Sn intermetallic compound (IMC) growth, and improve the fatigue resistance of the solder matrix. Consequently, SN100C can sustain cyclic stresses for a longer duration before reaching critical damage thresholds. However, the curve also shows that by the end of a 10-year mission profile, the majority of SN100C joints approach failure,

indicating that while superior to PB90SN10, this alloy still has limited long-term durability in harsh aerospace vibration conditions.

SAC305, on the other hand, demonstrates the most favorable performance among the three alloys. Its probability of failure curve remains well below that of both PB90SN10 and SN100C throughout the entire 10-year observation window, with less than 50% failure even after a decade of simulated vibration loading. This result can be explained by the superior mechanical and microstructural properties of the Sn–Ag–Cu system. SAC305 exhibits higher fracture toughness in mode I loading, improved ductility, and a fine, evenly distributed intermetallic compound network that enhances resistance against fatigue crack initiation. Furthermore, the Ag3Sn particles present in SAC305 act as strengthening phases, increasing the alloy's ability to withstand cyclic stresses without premature degradation. As a result, SAC305 offers the longest predicted lifetime and highest reliability in the considered BGA configuration.

It is important to note that this case study was performed solely on the BGA package configuration, with the primary aim of highlighting how solder alloy composition influences vibration fatigue life. The intention is not to provide a comprehensive comparative evaluation across all package types or environmental conditions, but rather to emphasize the necessity of considering solder alloy selection as a primary design parameter in reliability assessments. While the findings suggest that SAC305 is the superior candidate under the studied sinusoidal vibration profile, further work is needed to confirm its performance under random vibration, thermal cycling, and combined loading conditions. Additionally, experimental validation would provide deeper insights into damage mechanisms such as crack propagation paths, intermetallic compound morphology, and grain boundary effects, which were beyond the scope of this simulation-based analysis.

The probability of failure curves presented in Figure 10 underscore the significant role of solder alloy composition in determining the vibration fatigue lifetime of BGA interconnects. PB90SN10 demonstrates the shortest lifetime, with near-total failure within only a few years, while SN100C shows intermediate behavior with moderate fatigue resistance. SAC305 clearly outperforms both, offering a substantially longer operational lifespan and demonstrating the most robust resistance to sinusoidal vibration-induced fatigue. These findings reinforce the necessity of incorporating alloy selection into the early design and qualification phases of aerospace-grade electronics, where mission success is directly dependent on the long-term reliability of solder interconnects. Figure 30 illustrates the effect of solder alloy on the lifetime of the BGA package.

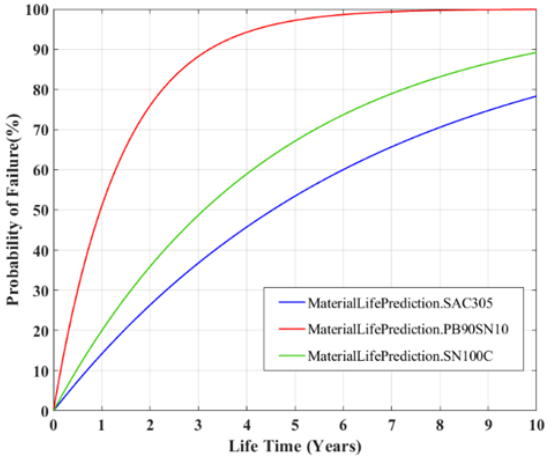

Figure 30. Effect of solder alloy on BGA lifetime

4.6 Predicting Board Failure under Dynamic Loading

In this study, variations in the failure rate of electronic boards under sinusoidal vibration loading are investigated using the bivariate Weibull distribution as a robust predictive and analytical model for failure behavior over time. This approach provides an effective and accurate means to simulate the impact of varying dynamic loading conditions on the failure process and crack propagation within electronic board components.

The bivariate Weibull distribution is a generalization of the conventional Weibull distribution, designed to model the joint behavior of two correlated random variables. This capability makes it particularly suitable for analyzing the performance of complex engineering systems influenced simultaneously by two primary factors, such as mechanical load intensity and time-dependent stress. By capturing the interactions between these variables, the bivariate model yields more realistic predictions of system reliability and failure progression compared to univariate approaches.

Traditionally, the Weibull distribution has been widely used to model time-to-failure data in engineering, as it accommodates various failure characteristics, including increasing, constant, or decreasing failure rates. In the bivariate context, the distribution models two interdependent random variables associated with system failure conditions, enabling a more comprehensive reliability analysis under dynamic vibrational environments.

The probability density function of the bivariate Weibull distribution can be expressed as follows:

$$F(t) = \frac{\beta}{\eta}\left(\frac{t}{\eta}\right)^{\beta-1} e^{-\left(\frac{t}{\eta}\right)^{\beta}} \quad (24)$$

Here, the Weibull shape parameter (β) is a critical statistical measure that characterizes the temporal distribution of failure events. This parameter also provides insight into the evolution of the failure rate over time; for example, a value of $\beta < 1$ indicates a decreasing

failure rate, whereas β > 1 corresponds to an increasing failure rate. Figure 28 illustrates the impact of varying the Weibull shape parameter on the estimated lifetime of the electronic board, highlighting how changes in β can significantly influence reliability predictions and maintenance planning. The results demonstrate the capability of the bivariate Weibull model to account for complex interactions between loading conditions and temporal effects, offering a valuable tool for predictive maintenance and reliability assessment in electronic systems. Figure 31 shows the effect of varying the Weibull slope on the estimated lifetime of the electronic board.

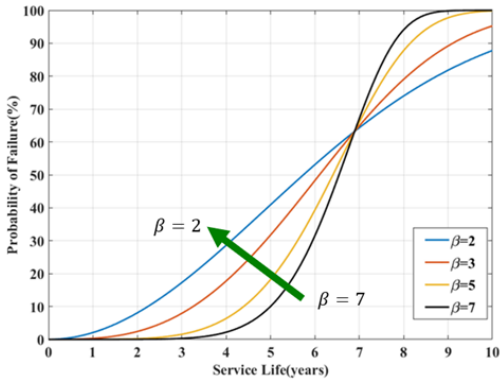

Figure 31. The effect of changing the Weibull slope on the estimated lifetime of the electronic board

4.7 Verification

The accuracy and credibility of the obtained FEM results and vibration-induced fatigue predictions were examined through a two-step verification and validation procedure. First, numerical verification was performed using a mesh-independence assessment, where the first three natural frequencies stabilized within approximately 2% once the mesh exceeded ~70,000 elements. This convergence confirms that the discretization is sufficiently refined to capture the stiffness distribution of the multilayer FR-4 PCB. Furthermore, the predicted first bending mode at 181 Hz shows close agreement with values reported for comparable multilayer PCB assemblies in the literature, including the modal characteristics documented by Tian et al. (2025) [52] and by Doranga et al. (2022) [54], thereby supporting the physical correctness of the adopted material properties and boundary conditions in ANSYS.

Since experimental vibration testing could not be performed in the present work, validation was achieved through comparison with established experimental trends in the literature. The simulated corner-ball failure tendency in BGA packages is consistent with the vibration-test observations of Baishya et al. (2022) [53] and the comprehensive review by Qiu et al. (2022) [55]. The FEM-predicted superior vibration endurance of leaded packages, arising from lead compliance and energy dissipation, also aligns with the experimental findings of Doranga et al. (2022) [54]. Similarly, the observed longer fatigue life of SAC305 relative to Sn-Pb and Sn-Cu alloys agrees with comparative material studies reported by Huang and Tee (2012) [56], who demonstrated improved viscoplastic durability of SAC-based alloys under dynamic loads. The substantial stress amplification under multi-axis excitation predicted in the present simulations matches the multi-directional vibration-induced failure behaviors described by Tian et al. (2025) [52]. Finally, the use of Dirlik and Tovo–Benasciutti models for wide-band fatigue estimation is supported by their validated performance across diverse random-vibration conditions as demonstrated by Benasciutti and Tovo (2005) [57].

Although exact numerical matching cannot be expected due to differences in geometry, solder alloy composition, PSD profiles, and mounting strategies, the strong consistency in failure locations, alloy-dependent fatigue rankings, package-level responses, and multi-axis stress amplification trends provides a solid literature-based validation of the present hybrid FEM–frequency-domain–Weibull methodology.

5. Conclusion

This study developed an integrated framework for evaluating vibration-induced fatigue and reliability of space-grade multilayer PCBs by combining finite element modeling (FEM), frequency-domain fatigue analysis, and two-parameter Weibull reliability estimation. Unlike previous works that examine vibration parameters in isolation, the proposed methodology simultaneously incorporates the coupled influence of vibration amplitude, multi-axial excitation, package geometry, and solder-alloy composition, addressing a key gap in aerospace electronics reliability.

The results show that component architecture strongly governs fatigue performance. Leaded packages demonstrated the highest vibration endurance, achieving roughly 2–3× longer life due to lead compliance, whereas BGA packages exhibited the shortest life because of corner-joint stress localization. LCCC components showed intermediate performance. Alloy selection also played a major role: SAC305 extended solder-joint life by up to 50% compared with PB90Sn10 and SN100C, confirming its suitability for high-frequency vibration conditions.

Multi-axial excitation significantly accelerated degradation, with tri-axial loading increasing equivalent von Mises stresses by 1.5–2× relative to uni-axial conditions. This highlights the inadequacy of traditional single-axis qualification tests and supports the adoption of multi-directional vibration profiles in standards such as MIL-STD-810 and NASA-GEVS. Coupling FEM stress predictions with Dirlik and Tovo–Benasciutti models provided accurate fatigue-damage estimates under wide-band random loading, while Weibull metrics (β ≈ 3–5)

enabled mission-relevant life measures such as MTTF and B10 life.

Design-level sensitivity analysis further showed that modifications to board geometry, component placement, mounting stiffness, high-Tg substrates, and protective coatings can reduce vibration stresses by 30–40%, offering practical strategies for improving reliability in harsh orbital environments.

Limitations include the absence of full experimental validation and incomplete modeling of combined thermo-vibrational fatigue. Future work should incorporate accelerated testing, machine-learning-assisted Weibull estimation, and evaluation of emerging lead-free alloys to enhance prediction accuracy. Overall, this research provides a unified physics-based and probabilistic framework for designing more reliable electronic assemblies for demanding aerospace missions.

Conflict of interest

The authors declare no conflicts of interest regarding this manuscript.

6. References

[1] T. Y. Tee, J. E. Luan, E. Pek, C. T. Lim, and Z. Zhong, "Advanced experimental and simulation techniques for analysis of dynamic responses during drop impact," *54th Electronic Components and Technology Conference*, Las Vegas, NV, USA, pp. 1088–1094, 2004, https://doi.org/10.1109/ECTC.2004.1319475.

[2] A. Goel and R. J. Graves, "Electronic system reliability: collating prediction models," *IEEE Transactions on Device and Materials Reliability*, vol. 6, no. 2, pp. 258–265, 2006, https://doi.org/10.1109/TDMR.2006.876570.

[3] E. Suhir, "Failure Oriented Accelerated Testing (FOAT) Boltzmann Arrnhenius Zhurkov Equation (BAZ) and their application in aerospace microelectronics and photonics reliability engineering," *International Journal of Aeronautical Science & Aerospace Research*, vol. 6, no. 3, pp. 185–191, 2019, https://doi.org/10.19070/2470-4415-1900022.

[4] J. Harikumaran, G. Buticchi, G. Migliazza, V. Madonna, P. Giangrande, and A. Costabeber, "Failure modes and reliability oriented system design for aerospace power electronic converters," *IEEE Open Journal of the Industrial Electronics Society*, vol. 2, pp. 53–64, 2021, https://doi.org/10.1109/OJIES.2020.3047201.

[5] Q. Xu, Y. Xu, P. Tu, T. Zhao, and P. Wang, "Systematic reliability modeling and evaluation for on-board power systems of more electric aircrafts," *IEEE Transactions on Power Systems*, vol. 34, no. 4, pp. 3264–3273, 2019, https://doi.org/10.1109/TPWRS.2019.2896454.

[6] H. Köck, S. Eiser, and M. Kaltenbacher, "Electrothermal multiscale modeling and simulation concepts for power electronics," *IEEE Transactions on Power Electronics*, vol. 31, no. 4, pp. 3128–3140, 2016, https://doi.org/10.1109/TPEL.2015.2453480.

[7] W. Engelmaier, "The use environments of electronic assemblies and their impact on surface mount solder attachment reliability," *Transactions on Components, Hybrids, and Manufacturing Technology*, vol. 13, no. 4, pp. 903–908, 1990, https://doi.org/10.1109/33.62538.

[8] K. Weide, "Impact of FEM simulation on reliability improvement of packaging," *Microelectronics Reliability*, vol. 39, no. 6–7, pp. 1079–1088, 1999, https://doi.org/10.1016/S0026-2714(99)00153-5.

[9] J. Depiver, S. Mallik, and E. H. Amalu, "Comparative analysis of SAC solder alloys for enhanced reliability in electronic assemblies: A finite element approach," *Microelectronics Reliability*, 2024, https://doi.org/10.21203/rs.3.rs-4755675/v1.

[10] W. Engelmaier, "Fatigue life of leadless chip carrier solder joints during power cycling," *IEEE Transactions on Components, Hybrids and Manufacturing Technology*, vol. 6, no. 3, pp. 232–237, 1983, https://doi.org/10.1109/TCHMT.1983.1136183.

[11] J. He, Y. Ling, and D. Lei, "Mechanical properties of Sn–Pb based solder joints and fatigue life prediction of PBGA package structure," *Ceramics International*, vol. 49, no. 16, pp. 27445–27456, 2023, https://doi.org/10.1016/j.ceramint.2023.06.017.

[12] A. M. Veprik and V. I. Babitsky, "Vibration protection of sensitive electronic equipment from harsh harmonic vibration," *Journal of Sound and Vibration*, vol. 238, no. 1, pp. 19–30, 2000, https://doi.org/10.1006/jsvi.2000.3098.

[13] L. Yang, F. Sun, H. Zhang, Z. Zhou, and Y. Qin, "Harmonic vibration test for accelerated reliability assessment of board level packaging," *7th International Forum on Strategic Technology (IFOST)*, Tomsk, Russia, pp. 1–5, 2012, https://doi.org/10.1109/IFOST.2012.6357731.

[14] F. Arabi, A. Gracia, J.-Y. Delétage, and H. Frémont, "Vibration test and simulation of printed circuit board," *19th International Conference on Thermal, Mechanical and Multi-Physics Simulation and Experiments in Microelectronics and Microsystems (EuroSimE)*, Toulouse, France, pp. 1–7, 2018, https://doi.org/10.1109/EuroSimE.2018.8369909.

[15] J. Tian, E. Shi, J. Zhong, Y. Chen, X. Deng, and G. Li, "Reliability analysis and structural optimization of circuit board based on vibration mode analysis and random vibration," *Processes*, vol. 12, no. 8, 2024, https://doi.org/10.3390/pr12081726.

[16] E. Suhir, "Response of a heavy electronic component to harmonic excitations applied to its external electric leads," *e & i Elektrotechnik und Informationstechnik*, vol. 124, no. 9, pp. 309–314, Sep. 2007, https://doi.org/10.1007/s00502-007-0458-z.

[17] J. Boiko, I. Kovtun, and S. Petrashchuk, "Vibration transmission in electronic packages having structurally complex design," *IEEE First Ukraine Conference on Electrical and Computer Engineering*, Kyiv, Ukraine, pp. 514–517, 2017, https://doi.org/10.1109/UKRCON.2017.8100294.

[18] K. Baishya, D. M. Harvey, T. P. Manzanera, G. Zhang, and D. R. Braden, "Failure patterns of solder joints identified through lifetime vibration tests," *Nondestructive Testing and Evaluation*, vol. 38, no. 1, pp. 147–171, 2023, https://doi.org/10.1080/10589759.2022.2084616.

[19] K.-W. Kim, J.-H. Park, T.-Y. Park, and H.-U. Oh, "Experimental evaluation of the effectiveness of the printed circuit board strain-based methodology in space-borne electronics with vertically mounted printed circuit boards," *Aerospace*, vol. 11, no. 7, p. 562, 2024, https://doi.org/10.3390/aerospace11070562.

[20] J. A. Depiver, S. Mallik, and E. H. Amalu, "Characterising solder materials from random vibration response of their interconnects in BGA packaging," *Journal of Electronic Materials*, vol. 52, no. 7, 2023, https://doi.org/10.1007/s11664-023-10394-x.

[21] W. Tian, F. Li, M. He, H. Ji, and S. Chen, "Reliability analysis of complex PCB assemblies under temperature cycling and random vibration," *Micromachines*, vol. 16, no. 2, p. 212, 2025, https://doi.org/10.3390/mi16020212.

[22] Z. Zhou, J. Chen, C. Yu, Y. Wang, and Y. Zhang, "Failure analysis of printed circuit board solder joint under thermal shock," *Coatings*, vol. 13, no. 3, p. 572, 2023, https://doi.org/10.3390/coatings13030572.

[23] T. T. Dele-Afolabi, M. N. M. Ansari, M. A. Hanim, A. A. Oyekanmi, O. J. Ojo-Kupoluyi, and A. Atiqah, "Recent advances in Sn-based lead-free solder interconnects for microelectronics packaging: Materials and technologies," *Journal of Materials Research and Technology*, vol. 25, pp. 4231–4263, 2023, https://doi.org/10.1016/j.jmrt.2023.06.193.

[24] J. A. Depiver, S. Mallik, and E. H. Amalu, "Finite element comparative study on creep and random vibrations of solder joints in BGA package," *power-electronic devices and components*, vol. 11, p. 100085, 2025, https://doi.org/10.1016/j.pedc.2025.100085.

[25] D. Bani Hani, R. Al Athamneh, M. Abueed, and S. Hamasha, "Reliability modeling of the fatigue life of lead-free solder joints at different testing temperatures and load levels using the Arrhenius model," *Scientific Reports*, vol. 13, no. 1, p. 2493, 2023, https://doi.org/10.1038/s41598-023-29636-3.

[26] E. G. Okafor, C. Ruby, M. Norris, A. Leda, and D. R. Huitink, "Sequential versus concurrent effects in combined stress solder joint reliability," *Journal of Electronic Packaging*, vol. 147, no. 2, p. 021002, 2025, https://doi.org/10.1115/1.4067189.

[27] E. Suhir, ""Quantifying the Unquantifiable" in aerospace electronics and ergonomics engineering: Review," *Journal of Aerospace Engineering and Mechanics*, vol. 4, pp. 306–347, 2020, https://doi.org/10.36959/422/449.

[28] B. Qiu, J. Xiong, H. Wang, S. Zhou, X. Yang, Z. Lin, M. Liu, and N. Cai, "Survey on fatigue life prediction of BGA solder joints," *Electronics*, vol. 11, no. 4, p. 542, 2022, https://doi.org/10.3390/electronics11040542.

[29] N. Muthuram and S. Saravanan, "Fatigue life based study of electronic package mounting locations on printed circuit boards subjected to random vibration loads," *Journal of Electronic Testing*, vol. 40, no. 6, pp. 761–776, 2024, https://doi.org/10.1007/s10836-024-06151-5.

[30] E. Bender, J. B. Bernstein, and D. S. Boning, "Modern trends in microelectronics packaging reliability testing," *Micromachines*, vol. 15, no. 3, p. 398, 2024, https://doi.org/10.3390/mi15030398.

[31] P. Borgesen, L. Wentlent, S. Hamasha, S. Khasawneh, S. Shirazi, D. Schmitz, T. Alghoul, C. Greene, and L. Yin, "A mechanistic thermal fatigue model for SnAgCu solder joints," *Journal of Electronic Materials*, vol. 47, no. 5, pp. 2526–2544, 2018, https://doi.org/10.1007/s11664-018-6121-0.

[32] M. Montazeri, "Combined stressors in reliability failure modes in flip-chip electronic packaging," M.S. thesis, University of Arkansas, 2021.

[33] J.-P. M. Clech, R. J. Coyle, and B. Arfaei, "Pb-free solder joint thermo-mechanical modeling: State of the art and challenges," *Journal of The Minerals, Metals & Materials Society*, vol. 71, no. 1, 2019, https://doi.org/10.1007/s11837-018-3003-0.

[34] D. Stone, "A study of the vibrational reliability performance of different doped low-creep lead-free solder paste and solder BGA packages," M.S. thesis, Auburn University, 2015.

[35] J. H. Lau and N.-C. Lee, Assembly and reliability of lead-free solder joints, Singapore: Springer, 2020, https://doi.org/10.1007/978-981-15-3920-6_6.

[36] F. X. Che and J. H. L. Pang, "Vibration reliability test and finite element analysis for flip chip solder joints," *Microelectronics Reliability*, vol. 49, no. 7, pp. 754–760, 2009, https://doi.org/10.1016/j.microrel.2009.03.022.

[37] M. A. Gharaibeh, "Reliability analysis of vibrating electronic assemblies using analytical solutions and response surface methodology," *Microelectronics Reliability*, vol. 84, pp. 238–247, 2018, https://doi.org/10.1016/j.microrel.2018.03.029.

[38] A. M. Veprik and V. I. Babitsky, "Vibration protection of sensitive electronic equipment from harsh harmonic vibration," *Journal of Sound and Vibration*, vol. 238, no. 1, pp. 19–30, 2000, https://doi.org/10.1006/jsvi.2000.3098.

[39] J. Tian, E. Shi, J. Zhong, Y. Chen, X. Deng, and G. Li, "Reliability analysis and structural optimization of circuit board based on vibration mode analysis and random vibration," *Processes*, vol. 12, no. 8, 2024, https://doi.org/10.3390/pr12081726.

[40] F. Arabi, A. Gracia, J.-Y. Delétage, and H. Frémont, "Vibration test and simulation of printed circuit board," *19th International Conference on Thermal, Mechanical and Multi-Physics Simulation and Experiments in Microelectronics and Microsystems (EuroSimE 2018)*, Toulouse, France, pp. 1–7, 2018, https://doi.org/10.1109/EuroSimE.2018.8369909.

[41] S. Doranga, M. Schuldt, and M. Khanal, "Effect of stiffening the printed circuit board in the fatigue life of the solder joint," *Materials*, vol. 15, no. 18, p. 6208, 2022, https://doi.org/10.3390/ma15186208.

[42] J. Mi, Y.-F. Li, Y.-J. Yang, W. Peng, and H.-Z. Huang, "Thermal cycling life prediction of Sn-3.0 Ag-0.5 Cu solder joint using Type-I censored data," *Scientific World Journal*, no. 1, p. 807693, 2014, https://doi.org/10.1155/2014/807693.

[43] W. Engelmaier, "Fatigue life of leadless chip carrier solder joints during power cycling," *IEEE Transactions On Components, Hybrids, And Manufacturing Technology*, vol. 6, no. 3, pp. 232–237, 2003, https://doi.org/10.1109/TCHMT.1983.1136183.

[44] J. He, Y. Ling, and D. Lei, "Mechanical properties of Sn–Pb based solder joints and fatigue life prediction of PBGA package structure," *Ceramics International*, vol. 49, no. 16, pp. 27445–27456, 2023, https://doi.org/10.1016/j.ceramint.2023.06.017.

[45] Q. Qasaimeh, H. Li, S. Hamasha, and J. Liu, "A machine learning framework with Shapley's additive explanations to assess solder joint reliability for electronic packaging," *Journal of Electronic Materials*, vol. 54, no. 9, pp. 7586–7608, 2025, https://doi.org/10.1007/s11664-025-12101-4.

[46] D. Bani Hani, R. Al Athamneh, M. Abueed, and S. Hamasha, "Reliability modeling of the fatigue life of lead-free solder joints at different testing temperatures and load levels using the Arrhenius model," *Scientific Reports*, vol. 13, no. 1, p. 2493, 2023, https://doi.org/10.1038/s41598-023-29636-3.

[47] E. G. Okafor, C. Ruby, M. Norris, A. Leda, and D. R. Huitink, "Sequential versus concurrent effects in combined stress solder joint reliability," *Journal of Electronic Packaging*, vol. 147, no. 2, p. 021002, 2025, https://doi.org/10.1115/1.4067189.

[48] E. Suhir, ""Quantifying the Unquantifiable" in aerospace electronics and ergonomics engineering: Review," *Journal of Aerospace Engineering and Mechanics*, vol. 4, pp. 306–347, 2020, https://doi.org/10.36959/422/449.

[49] W. Tian, F. Li, M. He, H. Ji, and S. Chen, "Reliability analysis of complex PCB assemblies under temperature cycling and random vibration," *Micromachines*, vol. 16, no. 2, p. 212, 2025, https://doi.org/10.3390/mi16020212.

[50] J. Xia, L. Yang, Q. Liu, Q. Peng, L. Cheng, and G. Li, "Comparison of fatigue life prediction methods for solder joints under random vibration loading," *Microelectronics Reliability*, vol. 95, pp. 58–64, 2019, https://doi.org/10.1016/j.microrel.2019.02.008.

[51] S. Su, F. J. Akkara, R. Thaper, A. Alkhazali, M. Hamasha, and S. Hamasha, "A state-of-the-art review of fatigue life prediction models for solder joint," *Journal of Electronic Packaging*, vol. 141, no. 4, p. 040802, 2019, https://doi.org/10.1115/1.4043405.

[52] W. Tian, F. Li, M. He, H. Ji, and S. Chen, "Reliability analysis of complex PCB assemblies under temperature cycling and random vibration," *Micromachines*, vol. 16, no. 2, p. 212, 2025, https://doi.org/10.3390/mi16020212.

[53] K. Baishya, D. M. Harvey, T. P. Manzanera, G. Zhang, and D. R. Braden, "Failure patterns of solder joints identified through lifetime vibration tests," *Nondestructive Testing and Evaluation*, vol. 38, no. 1, pp. 147–171, 2023, https://doi.org/10.1080/10589759.2022.2084616.

[54] S. Doranga, M. Schuldt, and M. Khanal, "Effect of stiffening the printed circuit board in the fatigue life of the solder joint," *Materials*, vol. 15, no. 18, p. 6208, 2022, https://doi.org/10.3390/ma15186208.

[55] B. Qiu, J. Xiong, H. Wang, S. Zhou, X. Yang, Z. Lin, M. Liu, and N. Cai, "Survey on fatigue life prediction of BGA solder joints," *Electronics*, vol. 11, no. 4, p. 542, 2022, https://doi.org/10.3390/electronics11040542.

[56] Qiu, B., J. Xiong, H. Wang, S. Zhou, X. Yang, Z. Lin, M. Liu, and N. Cai, "Survey on fatigue life prediction of BGA solder joints," *Electronics*, vol. 11, no. 4, p. 542, 2022, https://doi.org/10.3390/electronics11040542.

[57] D. Benasciutti and R. Tovo, "Spectral methods for lifetime prediction under wide-band stationary random processes," *International Journal of Fatigue*, vol. 27, no. 8, pp. 867–877, 2005, https://doi.org/10.1016/j.ijfatigue.2004.10.007.